Mass spectrum of spin-one hadrons in dense two-color QCD: Novel predictions by extended linear sigma model

Daiki Suenaga,[1,2,*] Kotaro Murakami,[3,4,†] Etsuko Itou,[4,5,‡] and Kei Iida[6,§]

[1]*Few-body Systems in Physics Laboratory, RIKEN Nishina Center, Wako 351-0198, Japan*
[2]*Research Center for Nuclear Physics, Osaka University, Ibaraki 567-0048, Japan*
[3]*Department of Physics, Tokyo Institute of Technology, 2-12-1 Ookayama, Megro, Tokyo 152-8551, Japan*
[4]*Interdisciplinary Theoretical and Mathematical Sciences Program (iTHEMS), RIKEN, Wako 351-0198, Japan*
[5]*Yukawa Institute for Theoretical Physics, Kyoto University, Kyoto 606-8502, Japan*
[6]*Department of Mathematics and Physics, Kochi University, 2-5-1 Akebono-cho, Kochi 780-8520, Japan*

(Received 14 January 2024; accepted 27 March 2024; published 30 April 2024)

We construct an extended version of the linear sigma model in such a way as to describe spin-1 hadrons as well as spin-0 hadrons in two-color QCD (QC_2D) by respecting the Pauli-Gürsey $SU(4)$ symmetry. Within a mean-field approximation, we therefrom examine a mass spectrum of the spin-1 hadrons at finite quark chemical potential (μ_q) and zero temperature. Not only mean fields of scalar mesons and scalar-diquark baryons but also of vector mesons and vector-diquark baryons are incorporated. As a result, we find that, unless all of those four types of mean fields are taken into account, neither lattice result for the critical μ_q that corresponds to the onset of baryon superfluidity nor for μ_q dependence of the pion mass can be reproduced. We also find that a slight suppression of the ρ meson mass in the superfluid phase, which was suggested by the lattice simulation, is reproduced by subtle mixing effects between spin-0 and spin-1 hadrons. Moreover, we demonstrate the emergence of an axial-vector condensed phase and possibly of a vector condensed phase by identifying the values of μ_q at which the corresponding hadron masses vanish. The possible presence of isotriplet 1^- diquarks that may be denoted by a tensor-type quark bilinear field is also discussed.

DOI: 10.1103/PhysRevD.109.074031

I. INTRODUCTION

Revealing the characteristics of hadrons in cold dense matter stands as a significant pursuit in quantum chromodynamics (QCD), since these particles serve as good probes to explore medium modifications of QCD symmetry properties, such as chiral symmetry restoration. For this reason, thus far, tremendous theoretical and experimental effort has been devoted to shed light on the hadronic properties in dense nuclear matter [1,2]. First-principles lattice Monte Carlo simulations, however, are difficult to apply to such a cold and dense regime due to the so-called sign problem [3,4]. Hence, our understanding of how the hadronic properties are modified in cold dense matter is limited as compared to the case of hot QCD matter.

Although lattice simulations remain to be effective in three-color QCD at finite quark chemical potential (μ_q), exceptionally for two-color QCD (QC_2D) with even numbers of quark flavors, the cumbersome sign problem disappears and indeed the simulations turn out to be applicable at nonzero μ_q [5]. So far, many lattice simulations have been performed toward the delineation of hadron modifications as well as of the phase structure in cold dense QC_2D [6–30] (see Ref. [31] and references therein). In concert with those numerical experiments, theoretical examinations have been made for qualitative understanding by using hadronic and microscopic models [32–60].

In QC_2D, diquarks, i.e., bound states of two quarks, emerge as color-singlet hadrons thanks to the pseudoreality of $SU(2)_c$ color group, unlike in three-color QCD. As a consequence, diquarks and mesons can be embedded into single multiplets and described collectively. Moreover, the pseudoreality allows us to extend $SU(2)_L \times SU(2)_R$ chiral symmetry to the so-called Pauli-Gürsey $SU(4)$ symmetry [32,33], and then, the chiral condensate induces the symmetry breaking of $SU(4) \to Sp(4)$. Thus, chiral models in

*daiki.suenaga@riken.jp
†kotaro.murakami@yukawa.kyoto-u.ac.jp
‡itou@yukawa.kyoto-u.ac.jp
§iida@kochi-u.ac.jp

QC_2D are constructed based on this symmetry-breaking pattern and, additionally, small violation of the Pauli-Gürsey $SU(4)$ symmetry to account for a finite pion mass.

Another noteworthy feature of QC_2D is the emergence of the diquark condensed phase; diquarks are bosonic hadrons carrying the quark number in QC_2D so that they start to form a Bose-Einstein condensate (BEC) at certain μ_q [32,33]. This distinctive phase violates $U(1)_B$ baryon-number symmetry spontaneously, and hence, the diquark condensed phase is also referred to as the baryon superfluid phase. Meanwhile, the stable phase at smaller μ_q, which no longer contains BECs, is simply called the hadronic phase. In the latter phase all thermodynamic quantities show no μ_q dependence at zero temperature, and such a salient property is called the Silver-Blaze property.

Recently, a mass spectrum of the low-lying spin-0 hadrons carrying negative and positive parities was simulated on lattice at finite μ_q [61,62]. The simulation result indicates that η mesons (isosinglet 0^- mesons) are lighter than pions in the superfluid phase, which is in contrast to our naive expectation that η mesons are heavier than pions due to the $U(1)_A$ anomaly effects. Motivated by this characteristic mass inversion, in Ref. [59] we constructed the linear sigma model (LSM) based on the (approximate) Pauli-Gürsey $SU(4)$ symmetry, which is capable of describing not only 0^- mesons and 0^+ (anti)diquark baryons but also 0^+ mesons and 0^- (anti)diquark baryons. Based on the LSM, indeed, we succeeded in explaining the mass inversion by showing that the η mass is sufficiently suppressed in the superfluid phase owing to mixing with 0^- (anti)diquark baryons, which is triggered by the $U(1)_B$ baryon-number violation.

In this paper, we extend the LSM by newly incorporating spin-1 hadrons, i.e., $1^\pm$ mesons and (anti)diquark baryons, but still respecting the Pauli-Gürsey $SU(4)$ symmetry. Then, we demonstrate the importance of mixing effects between spin-0 and spin-1 hadrons for the μ_q dependence of physical quantities such as the diquark condensate and the quark-number density. Besides, we present the predicted masses of spin-1 hadrons in cold matter and possible novel phases triggered by mass-vanishing spin-1 hadrons such as axial-vector and vector condensed phases.

The predictions given by the present study on how the spin-1 hadrons have their masses modified in cold matter are expected to be checked by future lattice QC_2D simulations. Ultimately, our comprehensive model, which allows us to simultaneously describe the spin-0 and spin-1 hadrons without incorporating the quark degrees of freedom explicitly, even at high densities, could serve as a guideline on how to use a hadronic model in cold matter. In addition, as diquarks themselves are observable, QC_2D possesses an advantage over three-color QCD where diquark dynamics can be solely seen through, e.g., singly heavy baryons (SHBs) made of one heavy quark and one diquark [63–71]. The SHBs are now under intensive investigation in accordance with the recent development of experimental techniques. In this regard, our findings on the diquarks in QC_2D would also serve as good references for understanding the SHBs dynamics from chiral symmetry.

This article is organized as follows. In Sec. II we introduce quark-bilinear fields for spin-0 and spin-1 hadrons and construct an effective model describing these hadrons based on the Pauli-Gürsey $SU(4)$ symmetry. After explaining, in Sec. III, our procedure to fix model parameters for later numerical calculations, we show, in Sec. IV, μ_q dependence of the mean fields within the present model and, in Sec. V, our main results, namely, the hadron mass spectrum at finite μ_q. Besides, the chiral partner structure for the spin-1 hadrons is demonstrated in Sec. VI. Sections VII and VIII are devoted to discussions and conclusions, respectively.

II. MODEL CONSTRUCTION

In this section, we construct our effective model describing both the spin-0 and spin-1 hadrons based on the linear realization of the Pauli-Gürsey $SU(4)$ symmetry.

A. Spin-0 hadron fields

For the purpose of constructing the effective Lagrangian, we first introduce a useful building block of the spin-0 hadrons whose $SU(4)$ symmetry properties are manifest, following the previous work [59].

In two-flavor QC_2D, $SU(2)_L \times SU(2)_R$ chiral symmetry is extended to the Pauli-Gürsey $SU(4)$ symmetry due to the pseudoreal property of $SU(2)_c$ gauge group, as shown in Appendix A. The extended symmetry enables us to treat mesons and diquark baryons in a unified way. Then, as shown in Ref. [59], it is useful to introduce a 4×4 matrix Σ corresponding to both the spin-0 mesons and diquarks baryons as defined by

$$\Sigma = \sum_{a=0}^{5} (\mathcal{S}^a + i\mathcal{P}^a) X^a E. \tag{1}$$

In this equation, $X^{a=0} = \frac{1}{2\sqrt{2}} \mathbf{1}_{4\times4}$ and $X^{a=1-5}$ are generators belonging to the Lie algebra of $SU(4)/Sp(4)$, the expressions for which are given by Eq. (B5) in Appendix B. Besides, E is the 4×4 symplectic matrix defined by

$$E = \begin{pmatrix} 0 & \mathbf{1}_f \\ -\mathbf{1}_f & 0 \end{pmatrix}. \tag{2}$$

In Eq. (1) $\mathcal{S}^a$ and $\mathcal{P}^a$ represent a set of the spin-0 hadron fields as

$$\sigma = \mathcal{S}^0, \qquad a_0^0 = \mathcal{S}^3, \qquad a_0^\pm = \frac{\mathcal{S}^1 \mp i\mathcal{S}^2}{\sqrt{2}},$$
$$\eta = \mathcal{P}^0, \qquad \pi^0 = \mathcal{P}^3, \qquad \pi^\pm = \frac{\mathcal{P}^1 \mp i\mathcal{P}^2}{\sqrt{2}},$$
$$B = \frac{\mathcal{S}^5 - i\mathcal{S}^4}{\sqrt{2}}, \qquad \bar{B} = \frac{\mathcal{S}^5 + i\mathcal{S}^4}{\sqrt{2}},$$
$$B' = \frac{\mathcal{P}^5 - i\mathcal{P}^4}{\sqrt{2}}, \qquad \bar{B}' = \frac{\mathcal{P}^5 + i\mathcal{P}^4}{\sqrt{2}}, \tag{3}$$

where σ, a_0, η, and π are mesons while B and B' ($\bar{B}$ and $\bar{B}'$) are (anti)diquark baryons. The quantum numbers carried by those hadrons are summarized in Table I. With the correspondence (3), the 4×4 matrix Σ reads,

$$\Sigma = \frac{1}{2}\begin{pmatrix} 0 & -B' + iB & \frac{\sigma - i\eta + a^0 - i\pi^0}{\sqrt{2}} & a^+ - i\pi^+ \\ B' - iB & 0 & a^- - i\pi^- & \frac{\sigma - i\eta - a^0 + i\pi^0}{\sqrt{2}} \\ -\frac{\sigma - i\eta + a^0 - i\pi^0}{\sqrt{2}} & -a^- + i\pi^- & 0 & -\bar{B}' + i\bar{B} \\ -a^+ + i\pi^+ & -\frac{\sigma - i\eta - a^0 + i\pi^0}{\sqrt{2}} & \bar{B}' - i\bar{B} & 0 \end{pmatrix}. \tag{4}$$

In terms of the quark doublet operator $\psi = (u, d)^T$, the hadrons are denoted by

$$\sigma \sim \bar{\psi}\psi, \qquad a_0^\pm \sim \frac{1}{\sqrt{2}}\bar{\psi}\tau_f^\mp\psi, \qquad a_0^0 \sim \bar{\psi}\tau_f^3\psi,$$
$$\eta \sim \bar{\psi}i\gamma_5\psi, \qquad \pi^\pm \sim \frac{1}{\sqrt{2}}\bar{\psi}i\gamma_5\tau_f^\mp\psi, \qquad \pi^0 \sim \bar{\psi}i\gamma_5\tau_f^3\psi,$$
$$B \sim -\frac{i}{\sqrt{2}}\psi^T\mathcal{C}\gamma_5\tau_c^2\tau_f^2\psi, \qquad B' \sim -\frac{1}{\sqrt{2}}\psi^T\mathcal{C}\tau_c^2\tau_f^2\psi,$$
$$\bar{B} \sim -\frac{i}{\sqrt{2}}\psi^\dagger\mathcal{C}\gamma_5\tau_c^2\tau_f^2\psi^*, \qquad \bar{B}' \sim \frac{1}{\sqrt{2}}\psi^\dagger\mathcal{C}\tau_c^2\tau_f^2\psi^*, \tag{5}$$

where $\mathcal{C} = i\gamma^2\gamma^0$ is the charge-conjugation Dirac matrix and $\tau_f^\pm = \tau_f^1 \pm i\tau_f^2$. Using Eqs. (3) and (5), one can see that, in terms of the four-component quark field Ψ defined by Eq. (A6), the 4×4 matrix Σ, Eq. (4), reads

TABLE I. Quantum numbers of the spin-0 hadrons.

Hadron	J^P	Quark number	Isospin
σ	0^+	0	0
a_0	0^+	0	1
η	0^-	0	0
π	0^-	0	1
B ($\bar{B}$)	0^+	+2 (−2)	0
B' ($\bar{B}'$)	0^-	+2 (−2)	0

$$\Sigma_{ij} \sim \Psi_j^T\sigma^2\tau_c^2\Psi_i. \tag{6}$$

Thus, under the $SU(4)$ transformation, Σ transforms as

$$\Sigma \to U\Sigma U^T \tag{7}$$

with $U \in SU(4)$. This symmetry property plays a significant role in constructing the effective Lagrangian describing the spin-0 hadrons.

Here, it is well-known that the sigma field (σ) can acquire its mean-field value; $\sigma_0 \equiv \langle\sigma\rangle$, to mimic the chiral condensate which results in the chiral symmetry breaking. Within such a mean-field level, the matrix (4) is reduced to

$$\Sigma \to \Sigma_0 \equiv \frac{\sigma_0}{2\sqrt{2}}E, \tag{8}$$

where E is the symplectic matrix, Eq. (2). In general, Σ_0 is not invariant under $SU(4)$: $\Sigma_0 \to U\Sigma_0 U^T$. Only when the element U is generated by h satisfying

$$hEh^T = E, \tag{9}$$

however, Σ_0 turns out to be invariant. Equation (9) shows that the spontaneous symmetry-breaking pattern triggered by the chiral condensate is $SU(4) \to Sp(4)$ in QC_2D.

Before moving on to the spin-1 hadrons, we comment on the properties of $\mathcal{S}^a$ and $\mathcal{P}^a$. With the correspondence (3), for instance, one can see that the pseudoscalar mesons (0^-) and scalar (anti)diquaks (0^+), parities of which are opposite, are collectively denoted by $\mathcal{P}^a$, i.e., these hadrons belong to the same multiplet of the $SU(4)$ algebra. The difference of parities are understandable from their intrinsic parities; the pseudoscalar mesons contain one quark and one antiquark while the scalar (anti)diquarks contain two (anti)quarks. Also, from this consideration it can be understood that those hadrons are the ground states in the hadronic phase because of their S wave nature in a quark-model description. Likewise, the scalar mesons (0^+) and pseudoscalar (anti)diquarks (0^-) are collectively represented by $\mathcal{S}^a$, while they belong to the same multiplet. Those hadrons can be identified as P-wave excited states.

B. Spin-1 hadron fields

In Sec. II A, we have introduced the 4×4 matrix Σ corresponding to the spin-0 mesons and diquark baryons. Next, in this subsection we consider another 4×4 matrix Φ^μ, which is essential to describe the spin-1 hadrons toward construction of our effective Lagrangian.

In two-flavor QC_2D, the relevant low-lying spin-1 mesons and diquark baryons are

$$\omega^\mu \sim \bar{\psi}\gamma^\mu\psi, \qquad f_1^\mu \sim \bar{\psi}\gamma_5\gamma^\mu\psi,$$
$$\rho^{0,\mu} \sim \bar{\psi}\tau_f^3\gamma^\mu\psi, \qquad \rho^{\pm,\mu} \sim \frac{1}{\sqrt{2}}\bar{\psi}\tau_f^{\mp}\gamma^\mu\psi,$$
$$a_1^{0,\mu} \sim \bar{\psi}\tau_f^3\gamma_5\gamma^\mu\psi, \qquad a_1^{\pm,\mu} \sim \frac{1}{\sqrt{2}}\bar{\psi}\tau_f^{\mp}\gamma_5\gamma^\mu\psi, \tag{10}$$

and

$$B_S^{I_z=0,\mu} \sim -\frac{i}{\sqrt{2}}\psi^T\mathcal{C}\gamma^\mu\tau_c^2\tau_f^1\psi$$
$$B_S^{I_z=\pm1,\mu} \sim -\frac{i}{2}\psi^T\mathcal{C}\gamma^\mu\tau_c^2(\mathbf{1}_f \pm \tau_f^3)\psi,$$
$$B_{AS}^\mu \sim -\frac{1}{\sqrt{2}}\psi^T\mathcal{C}\gamma_5\gamma^\mu\tau_c^2\tau_f^2\psi$$
$$\bar{B}_S^{I_z=0,\mu} = (B_S^{I_z=0,\mu})^\dagger, \qquad \bar{B}_S^{I_z=\pm1,\mu} = (B_S^{I_z=\mp1,\mu})^\dagger,$$
$$\bar{B}_{AS}^\mu = (B_{AS}^\mu)^\dagger, \tag{11}$$

respectively, in terms of the quark operator. The quantum numbers for those states are summarized in Table II. Here, for the spin-1 diquark baryons, the subscripts S and AS denote the "symmetric" and "antisymmetric" structure of the flavor contents, respectively, that is, the former is isotriplet while the latter is isosinglet. Besides, the superscript $I_z = 0, \pm1$ for B_S ($\bar{B}_S$) stands for the eigenvalues of the isospin "z components". We note that the axial-vector and vector (anti)diquark baryons are isotriplet and isosinglet, respectively, as dictated by the Pauli principle.[1]

TABLE II. Quantum numbers of the spin-1 hadrons.

Hadron	J^P	Quark number	Isospin
ω	1^-	0	0
ρ	1^-	0	1
f_1	1^+	0	0
a_1	1^+	0	1
B_S ($\bar{B}_S$)	1^+	+2 (−2)	1
B_{AS} ($\bar{B}_{AS}$)	1^-	+2 (−2)	0

For spin-1 hadrons, it would be convenient to introduce a 4×4 matrix Φ^μ by the following assignment:

$$\Phi^\mu = \frac{1}{2}\begin{pmatrix} \frac{\omega+\rho^0-(f_1+a_1^0)}{\sqrt{2}} & \rho^+ - a_1^+ & \sqrt{2}B_S^{I_z=+1} & B_S^{I_z=0} - B_{AS} \\ \rho^- - a_1^- & \frac{\omega-\rho^0-(f_1-a_1^0)}{\sqrt{2}} & B_S^{I_z=0} + B_{AS} & \sqrt{2}B_S^{I_z=-1} \\ \sqrt{2}\bar{B}_S^{I_z=-1} & \bar{B}_S^{I_z=0} + \bar{B}_{AS} & -\frac{\omega+\rho^0+f_1+a_1^0}{\sqrt{2}} & -(\rho^- + a_1^-) \\ \bar{B}_S^{I_z=0} - \bar{B}_{AS} & \sqrt{2}\bar{B}_S^{I_z=+1} & -(\rho^+ + a_1^+) & -\frac{\omega-\rho^0+f_1-a_1^0}{\sqrt{2}} \end{pmatrix}^\mu. \tag{12}$$

In fact, in terms of the four-component quark field Ψ, Eq. (A6), and the interpolating fields, Eqs. (10) and (11), Φ^μ can be simply rewritten in the form of

$$\Phi_{ij} \sim \Psi_j^\dagger\sigma^\mu\Psi_i, \tag{13}$$

where $\sigma^\mu = (\mathbf{1}, \sigma^i)$ (σ^i is the Pauli matrix in the two-component spinor space). Thus, the matrix (12) fulfills the following homogeneous $SU(4)$ transformation law:

$$\Phi^\mu \to U\Phi^\mu U^\dagger, \tag{14}$$

which allows us to construct an effective Lagrangian straightforwardly. For this reason, in what follows we employ Φ^μ as a building block of the spin-1 hadrons. We note that, with the help of $U(4)$ generators X^a and S^i, Eqs. (B5) and (B4), the spin-1 hadron matrix Φ^μ can be expressed as

$$\Phi^\mu = \left(\sum_{i=1}^{10} V^i S^i - \sum_{a=0}^{5} V'^a X^a\right)^\mu, \tag{15}$$

where

$$\omega = V^0, \qquad \rho^\pm = \frac{V^1 \mp iV^2}{\sqrt{2}}, \qquad \rho^0 = V^3,$$
$$f_1 = V'^0, \qquad a_1^\pm = \frac{V'^1 \mp iV'^2}{\sqrt{2}}, \qquad a_1^0 = V'^3,$$
$$B_S^{I_z=0} = \frac{V^9 + iV^{10}}{\sqrt{2}}, \qquad \bar{B}_S^{I_z=0} = \frac{V^9 - iV^{10}}{\sqrt{2}},$$
$$B_S^{I_z=\pm1} = \frac{(V^5 + iV^6) \pm (V^7 + iV^8)}{2},$$
$$\bar{B}_S^{I_z=\pm1} = \frac{(V^5 - iV^6) \mp (V^7 - iV^8)}{2},$$
$$B_{AS} = \frac{V'^5 - iV'^4}{\sqrt{2}}, \qquad \bar{B}_{AS} = \frac{V'^5 + iV'^4}{\sqrt{2}}. \tag{16}$$

The reduced form (15) is useful to see symmetry properties of the spin-1 hadrons. For instance, from

[1]In three-color QCD, the diquarks are translated into SHBs. Indeed, the axial-vector and vector diquarks, B_S and B_{AS}, would correspond to $\Sigma_c(2455)$ [and its heavy-quark spin partner $\Sigma_c(2520)$] and $\Lambda_c(2595)$ [and $\Lambda_c(2625)$], respectively.

Eq. (15) one can see that the vector mesons (1^-) and axial-vector (anti)diquarks (1^+), parities of which are opposite, belong to the $Sp(4)$ algebra proportional to S^i and hence to the same multiplet. Likewise, the axial-vector mesons (1^+) and vector (anti)diquarks (1^-) are the elements of the remaining algebra. The difference of parities between the mesons and (anti)diquarks in a single multiplet can be understood from their intrinsic parities as in the case of the spin-0 hadrons. We note that V^i and V'^a are the ground and excited states, respectively, in the hadronic phase, since the former and latter are identifiable as S-wave and P-wave states, respectively.

C. Extended linear sigma model

In Sec. II A and Sec. II B, the 4×4 matrices corresponding to the spin-0 and spin-1 hadrons in two-flavor QC_2D, Σ and Φ^μ, have been introduced. In this subsection, by making the most of these building blocks, we construct an effective Lagrangian to describe interactions among those hadrons.

The $SU(4)$ transformation laws for Σ and Φ^μ are given by Eqs. (7) and (14). Toward construction of the effective Lagrangian, in addition to the $SU(4)$ properties it is necessary to examine the discrete symmetries; parity and charge conjugation invariance. Those discrete transformation laws of Σ and Φ^μ can be read off from the interpolating fields (6) and (13). From Eq. (A6) the four-component quark field Ψ transforms as

$$\Psi(x)\overset{\mathcal{P}}{\to}\Omega\tau_c^2\sigma^2\Psi^*(x_P),\qquad \Psi\overset{\mathcal{C}}{\to} iE^T\tau^2\Psi, \tag{17}$$

under parity and charge conjugation with $x_P=(x^0,-\boldsymbol{x})$, where E is the symplectic matrix (2) and Ω is defined by

$$\Omega=\begin{pmatrix}0 & \mathbf{1}_f\\ \mathbf{1}_f & 0\end{pmatrix}. \tag{18}$$

Thus, the resultant transformation laws of Σ and Φ^μ read

$$\begin{aligned}&\Sigma(x)\overset{\mathcal{P}}{\to}\Omega\Sigma^\dagger(x_P)\Omega, && \Sigma\overset{\mathcal{C}}{\to}E^T\Sigma E,\\ &\Phi^\mu(x)\overset{\mathcal{P}}{\to}-\Omega\Phi_\mu^T(x_P)\Omega, && \Phi^\mu\overset{\mathcal{C}}{\to}E^T\Phi^\mu E.\end{aligned} \tag{19}$$

Using the transformation laws given by Eqs. (7), (14), and (19), one can construct the following effective Lagrangian in such a way as to preserve the Pauli-Gürsey $SU(4)$ symmetry as well as parity and charge-conjugation invariance:

$$\begin{aligned}\mathcal{L}_{\rm eLSM}=&\,\mathrm{tr}[D_\mu\Sigma^\dagger D^\mu\Sigma]-m_0^2\mathrm{tr}[\Sigma^\dagger\Sigma]-\lambda_1(\mathrm{tr}[\Sigma^\dagger\Sigma])^2-\lambda_2\mathrm{tr}[(\Sigma^\dagger\Sigma)^2]+\mathrm{tr}[H^\dagger\Sigma+\Sigma^\dagger H]+c(\det\Sigma+\det\Sigma^\dagger)\\&-\frac{1}{2}\mathrm{tr}[\Phi_{\mu\nu}\Phi^{\mu\nu}]+m_1^2\mathrm{tr}[\Phi_\mu\Phi^\mu]+ig_3\mathrm{tr}[\Phi_{\mu\nu}[\Phi^\mu,\Phi^\nu]]+h_1\mathrm{tr}[\Sigma^\dagger\Sigma]\mathrm{tr}[\Phi_\mu\Phi^\mu]+h_2\mathrm{tr}[\Sigma\Sigma^\dagger\Phi_\mu\Phi^\mu]\\&+h_3\mathrm{tr}[\Phi_\mu^T\Sigma^\dagger\Phi^\mu\Sigma]+g_4\mathrm{tr}[\Phi_\mu\Phi_\nu\Phi^\mu\Phi^\nu]+g_5\mathrm{tr}[\Phi_\mu\Phi^\mu\Phi_\nu\Phi^\nu]+g_6\mathrm{tr}[\Phi_\mu\Phi^\mu]\mathrm{tr}[\Phi_\nu\Phi^\nu]+g_7\mathrm{tr}[\Phi_\mu\Phi_\nu]\mathrm{tr}[\Phi^\mu\Phi^\nu].\end{aligned} \tag{20}$$

In this Lagrangian,

$$\Phi_{\mu\nu}\equiv D_\mu\Phi_\nu-D_\nu\Phi_\mu \tag{21}$$

is the field strength of Φ^μ and the covariant derivatives read,

$$\begin{aligned}&D_\mu\Sigma\equiv\partial_\mu\Sigma-iG_\mu\Sigma-i\Sigma G_\mu^T-ig_1\Phi_\mu\Sigma-ig_2\Sigma\Phi_\mu^T,\\&D_\mu\Phi_\nu\equiv\partial_\mu\Phi_\nu-i[G_\mu,\Phi_\nu],\end{aligned} \tag{22}$$

where G_μ is an external field, the transformation law of which is $G_\mu\to UG_\mu U^\dagger-i\partial_\mu UU^\dagger$. One systematic way to introduce the chemical potential μ_q is to replace the time component of the $U(1)_B$ baryon-number part of G_μ appropriately. Here, from Eq. (A8) and the interpolating fields (6) and (13), the $U(1)_B$ baryon-number part is proportional to J defined by

$$J\equiv\begin{pmatrix}\mathbf{1}_f & 0\\ 0 & -\mathbf{1}_f\end{pmatrix}. \tag{23}$$

Hence, we replace G_μ by

$$G_\mu\to\mu_q\delta_{\mu0}J, \tag{24}$$

to access a finite-density system. Besides, in constructing the model, we have included contributions allowed by the relevant symmetries up to fourth order in $\Sigma^{(\dagger)}$ and Φ^μ. We note that the 4×4 matrix H in Eq. (20) is responsible for explicit breaking of the Pauli-Gürsey $SU(4)$ symmetry to yield the finite pion mass, which takes the form of

$$H=h_qE. \tag{25}$$

The Lagrangian (20) can be understood as an extension of the previous LSM established in Ref. [59] where only spin-0 hadrons are treated. For this reason we call this model the extended linear sigma model (eLSM). We note that this eLSM is the QC_2D version of the one invented for three-color QCD by the Frankfurt group [72] and applied to the case of finite density by one of the present authors [73].

In the eLSM Lagrangian (20), with the help of the antisymmetric property: $\Sigma^T=-\Sigma$, the kinetic term for Σ can be expanded as

$$\begin{aligned}\mathrm{tr}[D_\mu\Sigma^\dagger D^\mu\Sigma] &= \mathrm{tr}[\partial_\mu\Sigma^\dagger\partial^\mu\Sigma] + (g_1+g_2)\mathrm{tr}[\Sigma\Sigma^\dagger(\Phi_\mu G^\mu \\ &\quad + G_\mu\Phi^\mu)] + 2(g_1+g_2)\mathrm{tr}[\Phi_\mu^T\Sigma^\dagger G^\mu\Sigma] \\ &\quad + i(g_1+g_2)\mathrm{tr}[\Phi_\mu(\partial^\mu\Sigma\Sigma^\dagger - \Sigma\partial^\mu\Sigma^\dagger)] \\ &\quad + (g_1^2+g_2^2)\mathrm{tr}[\Sigma\Sigma^\dagger\Phi_\mu\Phi^\mu] \\ &\quad + 2g_1g_2\mathrm{tr}[\Phi_\mu^T\Sigma^\dagger\Phi^\mu\Sigma]. \end{aligned} \tag{26}$$

The trace structure of the last two pieces in the right-hand side is equivalent to the h_2 and h_3 terms in Eq. (20), while the remaining interactions are proportionally dependent on the combination of g_1+g_2 alone. Hence, the four parameters g_1, g_2, h_2, and h_3 can be absorbed into three new combinations,

$$\begin{aligned} C_1 &\equiv g_1+g_2, \\ C_2 &\equiv g_1^2+g_2^2+h_2, \\ C_3 &\equiv 2g_1g_2+h_3. \end{aligned} \tag{27}$$

When the spectrum includes spin-1 hadrons, it is well-known that the Zweig rule, i.e., the large N_c suppression of the interactions, works phenomenologically. In other words, diagrams that are not linked by a single quark line are not expected to play significant roles as far as the spin-1 hadrons are concerned. In the following analysis, therefore, we will leave only terms including a single trace for Φ^μ's, which allows us to work with the following reduced eLSM:

$$\begin{aligned}\mathcal{L}_{\mathrm{eLSM}}^{\mathrm{red}} &= \mathrm{tr}[D_\mu\Sigma^\dagger D^\mu\Sigma] - m_0^2\mathrm{tr}[\Sigma^\dagger\Sigma] - \lambda_1(\mathrm{tr}[\Sigma^\dagger\Sigma])^2 - \lambda_2\mathrm{tr}[(\Sigma^\dagger\Sigma)^2] + \mathrm{tr}[H^\dagger\Sigma + \Sigma^\dagger H] + c(\det\Sigma + \det\Sigma^\dagger) - \frac{1}{2}\mathrm{tr}[\Phi_{\mu\nu}\Phi^{\mu\nu}] \\ &\quad + m_1^2\mathrm{tr}[\Phi_\mu\Phi^\mu] + ig_3\mathrm{tr}[\Phi_{\mu\nu}[\Phi^\mu,\Phi^\nu]] + h_2\mathrm{tr}[\Sigma\Sigma^\dagger\Phi_\mu\Phi^\mu] + h_3\mathrm{tr}[\Phi_\mu^T\Sigma^\dagger\Phi^\mu\Sigma] + g_4\mathrm{tr}[\Phi_\mu\Phi_\nu\Phi^\mu\Phi^\nu] \\ &\quad + g_5\mathrm{tr}[\Phi_\mu\Phi^\mu\Phi_\nu\Phi^\nu]. \end{aligned} \tag{28}$$

As we will see, the masses of the hadrons can be read off from quadratic terms of the corresponding fields on top of the appropriate mean fields.

III. INPUTS

In Sec. II C we have constructed the eLSM to describe both the spin-0 and spin-1 hadrons at arbitrary μ_q. In this section, before numerical investigation of μ_q dependence of the mean fields and the hadron masses, we explain our procedure to determine various parameters of the reduced eLSM.

The reduced eLSM (28) includes 12 parameters; m_0^2, m_1^2, λ_1, λ_2, h_q, c, g_3, g_4, g_5, C_1, C_2, and C_3. In this exploratory study, we try to reduce the number of the parameters as much as possible to avoid unnecessary complexities in the following numerical analysis. First, as discussed in Ref. [59], contributions from the λ_1 and c terms, which only affect the mass spectrum of the spin-0 hadrons, are expected to be small from the N_c counting. Thus, we take $\lambda_1 = c = 0$. The main aim of the present paper is to delineate the behavior of the spin-1 hadrons at finite μ_q, so that this simplification does not affect the following arguments considerably. Next, as for the couplings among the spin-1 hadrons, there is no *a priori* way to determine all of the parameters due to the currently limited lattice data. When we derive the present eLSM from the $\mathcal{O}(p^2)$ hidden-local-symmetry (HLS) Lagrangian [41], however, it is expected that the interactions among the spin-1 hadrons satisfy the following "gauge-principle parametrization":

$$g_3 = g_\Phi, \qquad g_4 = -g_5 = g_\Phi^2. \tag{29}$$

From this consideration, we assume Eq. (29) to employ only a single parameter g_Φ instead of g_3, g_4, and g_5. In addition, one can see from Eq. (27) that the roles of C_1, C_2, and C_3 are essentially the same; these three parameters control the interaction strength between the spin-0 and spin-1 hadrons. For this reason we assume

$$C_1 = C_2 \equiv C \tag{30}$$

for simplicity. In Eq. (30) we have not included C_3 to define the common coupling, since C_3 is uniquely fixed by inputs as will be explained below.

Now the number of the model parameters is reduced to seven: m_0^2, m_1^2, λ_2, h_q, g_Φ, C, and C_3. The present study is devoted to unveiling properties of the spin-1 hadrons, and hence, we take C and g_Φ, which control couplings related to the spin-1 hadrons, as free parameters. In order to determine the remaining five parameters, as the first four inputs, we use the masses of π, $B'(\bar{B}')$, ρ, and a_1 at vanishing μ_q simulated in Refs. [61,62]. In these lattice simulations, the mass ratio of the pion and the ρ meson reads $m_\pi^{(\mathrm{H})}/m_\rho^{(\mathrm{H})} \approx 0.81$.[2] When we fix the physics scale such that the pseudocritical temperature of the chiral phase transition becomes $T_c = 200$ MeV at $\mu_q = 0$ [24], the input mass values are given by [61,62]

$$\begin{aligned} m_\pi^{(\mathrm{H})} &= 738\ \mathrm{MeV}, & m_{B'(\bar{B}')}^{(\mathrm{H})}\Big|_{\mu_q=0} &= 1611\ \mathrm{MeV}, \\ m_\rho^{(\mathrm{H})} &= 908\ \mathrm{MeV}, & m_{a_1}^{(\mathrm{H})} &= 1614\ \mathrm{MeV}. \end{aligned} \tag{31}$$

[2]The superscript (H) is attached to emphasize that the quantities are defined in the hadronic phase where no diquark condensates emerge.

While the pion mass is considerably heavier than the physical value, we employ these inputs in the present work to consistently provide predictions for future lattice simulations. As for the last input, following Ref. [59] we take the mean field value of σ as

$$\sigma_0^{(\mathrm{H})} = 250\ \mathrm{MeV}, \tag{32}$$

which gives a typical strength of the chiral symmetry breaking. Using analytic expressions for the hadron masses derived in Appendix D, together with Eqs. (31) and (32), the remaining parameters can finally be determined as

$$\begin{aligned} m_0^2 &= -\frac{1}{2}[(m_{a_0}^{(\mathrm{H})})^2 - 3Z_\pi^{-2}(m_\pi^{(\mathrm{H})})^2], \\ m_1^2 &= \frac{1}{2}[(m_\rho^{(\mathrm{H})})^2 + (m_{a_1}^{(\mathrm{H})})^2] - \frac{C}{8}(\sigma_0^{(\mathrm{H})})^2, \\ \lambda_2 &= \frac{2}{(\sigma_0^{(\mathrm{H})})^2}[(m_{a_0}^{(\mathrm{H})})^2 - Z_\pi^{-2}(m_\pi^{(\mathrm{H})})^2], \\ h_q &= \frac{\sigma_0^{(\mathrm{H})}}{2\sqrt{2}} Z_\pi^{-2}(m_\pi^{(\mathrm{H})})^2, \\ C_3 &= \frac{4}{(\sigma_0^{(\mathrm{H})})^2}[(m_{a_1}^{(\mathrm{H})})^2 - (m_\rho^{(\mathrm{H})})^2], \end{aligned} \tag{33}$$

for a given C, where the renormalization factor Z_π is of the form

$$Z_\pi = \left(1 - \frac{C^2(\sigma_0^{(\mathrm{H})})^2}{8(m_{a_1}^{(\mathrm{H})})^2}\right)^{-1/2}. \tag{34}$$

We note that the analytic expression for h_q, which links the magnitude of explicit breaking of chiral symmetry to the pion mass, can be derived from a stationary condition of the effective potential with respect to $\sigma_0^{(\mathrm{H})}$.

In the following analysis, we will regard g_Φ and C as free parameters to explore how the mean fields as well as hadron masses behave at finite μ_q. Recall that g_Φ is the coupling constant that controls the interaction strength among only spin-1 hadrons. Meanwhile, C is particularly responsible for the transition between the spin-0 and spin-1 hadrons through derivative couplings, as indicated by Eq. (26). Thus, C can be regarded as a parameter that measures the magnitude of the spin-0 and spin-1 mixing effect. For instance, in the hadronic phase, nonzero C induces π—a_1 mixing and η—f_1 mixing, which can be captured by the renormalization constants, Z_π and Z_η, as derived in Appendix D.

IV. MEAN FIELDS

In this section, employing a mean-field approximation, we numerically explore μ_q dependence of the mean fields at zero temperature from the reduced eLSM (28) with the inputs presented in Sec. III.

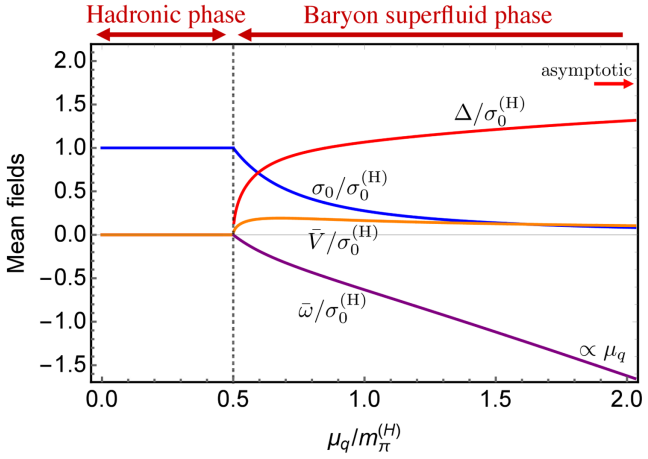

FIG. 1. μ_q dependence of the mean fields: σ_0, Δ, $\bar{\omega}$, and $\bar{V}$, with $C = 12$. The value indicated by the arrow represents the asymptotic constant value of Δ; $\Delta \sim 0.34 m_1 = 1.74\sigma_0^{(\mathrm{H})}$.

At finite μ_q, not only the sigma meson σ but also the (anti)diquark baryon B ($\bar{B}$) can acquire a nonzero mean-field value, resulting in the appearance of the baryon superfluid phase [32,33]. Following Ref. [59] we take $\Delta \equiv \langle B^5 \rangle$ to express the mean field of the (anti)diquark. In addition to those spin-0 hadrons, violation of the Lorentz invariance yields a mean field of the ω meson [74]. Assuming the parity invariance, only the time component of ω can have a nonzero mean-field value: $\bar{\omega} \equiv \langle \omega_{\mu=0} \rangle$. Furthermore, in the baryon superfluid phase, one can expect that the ω meson mixes with the vector (anti)diquark B_{AS} ($\bar{B}_{AS}$) due to the baryon-number violation. Thus, these diquarks are also capable of acquiring nonzero mean-field values. When the phase of Δ is chosen according to $\Delta = \langle B^5 \rangle$, only $\bar{V} \equiv \langle V'^4_{\mu=0} \rangle$ becomes nonzero.[3] To summarize, in the present analysis we take into account the following four mean fields without loss of generality:

$$\begin{aligned} \sigma_0 &= \langle \sigma \rangle, & \Delta &= \langle B^5 \rangle, \\ \bar{\omega} &= \langle \omega_{\mu=0} \rangle, & \bar{V} &\equiv \langle V'^4_{\mu=0} \rangle. \end{aligned} \tag{35}$$

The μ_q dependence of these mean fields can be determined by solving the corresponding stationary conditions.

Depicted in Fig. 1 is the resultant μ_q dependence of the mean fields: σ_0, Δ, $\bar{\omega}$, and $\bar{V}$, normalized by $\sigma_0^{(\mathrm{H})}$. In obtaining this plot, the strength of the spin-0 and spin-1 mixing effect is chosen as $C = 12$. As shown in Sec. V B,

[3]In this phase choice, one can indeed prove that $\langle V'^5_{\mu=0} \rangle$ must be always zero by solving the stationary conditions explicitly. Inversely, if we choose the phase of Δ such that $\langle B^4 \rangle \neq 0$ but $\langle B^5 \rangle = 0$, then $\langle V'^4_{\mu=0} \rangle = 0$ but $\langle V'^5_{\mu=0} \rangle \neq 0$ is obtained for $\bar{V}$.

this value leads to a slight reduction of the ρ mass in the superfluid phase, a feature consistent with the lattice data [61,62]. We note that the stationary conditions hold independently of g_Φ, so that the resultant μ_q dependence of the mean fields is not affected by g_Φ. Figure 1 implies that the baryon superfluid phase is triggered by the onset of nonzero Δ at a critical chemical potential $\mu_q = \mu_q^{\rm cr}$ with

$$\mu_q^{\rm cr} \equiv m_\pi^{\rm (H)}/2, \tag{36}$$

which is irrespective of whether or not the spin-1 hadrons are present. This critical value is universal in the sense that it is also derived from chiral effective models involving only spin-0 hadrons [32,33,36,59]. At the same time as the onset, both $\bar{V}$ and $\bar{\omega}$ begin to acquire nonzero values. Detailed analyses in the vicinity of the phase transition will be provided in Sec. VII A. At asymptotically high μ_q, σ_0 and $\bar{V}$ vanish. Meanwhile, Δ converges to a constant (see the arrow in Fig. 1) whose value can be evaluated as $\Delta/\sigma_0^{\rm (H)} \approx 0.34(m_1/\sigma_0^{\rm (H)}) = 1.74$ for the present values of C and C_3, whereas $\bar{\omega}$ grows in the negative direction with a power of μ_q.

Here, we note that the onsets of nonzero $\bar{\omega}$ and $\bar{V}$ do not necessarily coincide with the critical chemical potential (36), since those mean fields are unphysical, in other words, they are gauge-dependent quantities within the gauge-field description. In fact, the mean field of ω was found to be proportional to μ_q in the hadronic phase within the HLS formalism [41].

The converging behavior of Δ is distinct from the result within the conventional LSM in the absence of spin-1 hadrons [59]. To take a closer look at this difference, we depict the μ_q dependence of σ_0 and Δ with and without the spin-0 and spin-1 mixing effect, $C = 12$ and $C = 0$, in the top panel of Fig. 2. The figure indicates that σ_0 does not have its μ_q dependence corrected considerably by the mixing while Δ has its μ_q dependence significantly modified by the mixing; the asymptotically converging behavior of Δ is induced only when the spin-0 and spin-1 mixing takes effect. In fact, the asymptotic constant value of Δ with the mixing effect is essentially determined by the bare mass of the spin-1 hadrons, m_1, together with a factor stemming from the mixing strength C and C_3. The diverging behavior of Δ in the absence of the mixing is lost, but instead the negatively diverging growth of $\bar{\omega}$ appears as indicated in Fig. 1. We note that spin-1 mean fields $\bar{\omega}$ and $\bar{V}$ are always zero when $C = 0$,

$$\bar{\omega} = 0 \quad \text{and} \quad \bar{V} = 0 \quad (\text{at any } \mu_q \text{ for } C = 0), \tag{37}$$

as will be argued in Sec. VII A. We also note that, when we take C to be negative, the signs of the induced $\bar{\omega}$ and $\bar{V}$ in the superfluid phase become positive and negative, respectively.

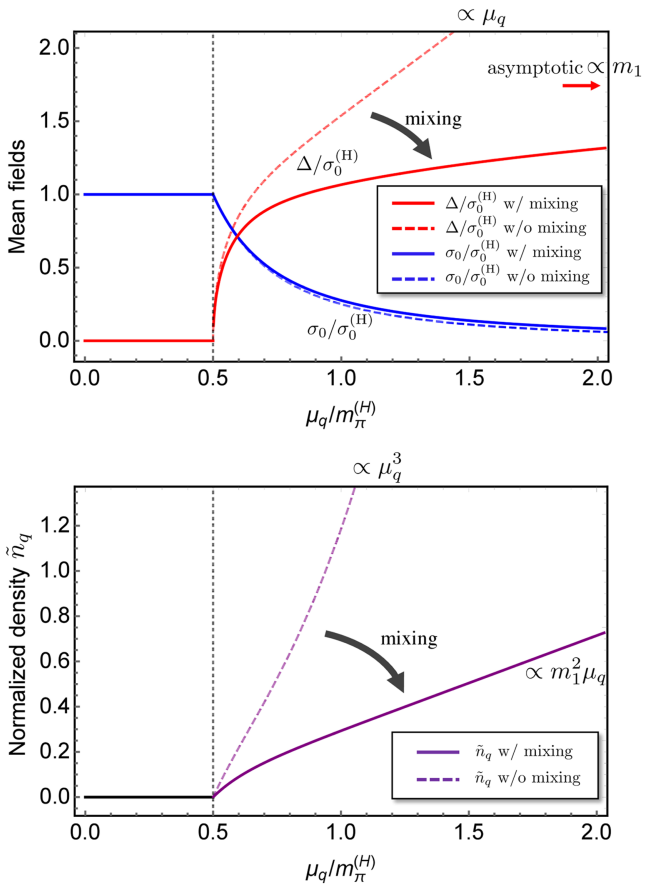

FIG. 2. μ_q dependence of σ_0 and Δ (top) and of the quark-number density $\tilde{n}_q$ (bottom) with and without spin-0 and spin-1 mixing, $C = 12$ and $C = 0$.

The emergence of $\bar{\omega}$ induced by the mixing makes the growth of Δ suppressed everywhere in the superfluid phase. Here, we recall that in three-color QCD, the repulsive contributions from ω mesons play a significant role in stabilizing nuclear matter against the attractive ones from σ mesons [74]. In this regard, the hindered evolution of Δ in the present $\mathrm{QC_2D}$ matter would also be understood by such repulsive effects.[4]

The significant corrections due to the spin-0 and spin-1 mixing effect are also reflected by μ_q dependence of the quark-number density as displayed in the bottom panel of Fig. 2. In this figure we have plotted the normalized density

$$\tilde{n}_q = \frac{n_q}{16 f_\pi^2 m_\pi^{\rm (H)}}, \tag{38}$$

where n_q is the ordinary quark-number density given by

[4]For another notable effect of $\bar{\omega}$, this mean field will be found to suppress the chemical potential of the diquark baryons effectively as $2\mu_q \to 2\mu_q + (C/2\sqrt{2})\bar{\omega}$ with $(C/2\sqrt{2})\bar{\omega} < 0$, as shown in, e.g., Eq. (C16). This negative effect is consistent with the case for nucleons in three-color QCD.

$$n_q = \left.\frac{\partial \mathcal{L}^{\text{red.}}_{\text{eLSM}}}{\partial \mu_q}\right|_{\text{mean field}} = 4\Delta^2\mu_q + \frac{C\Delta}{\sqrt{2}}(\Delta\bar{\omega} - \bar{V}\sigma_0) \quad (39)$$

with the mean fields (35), and $f_\pi = \sigma_0^{(\text{H})}/\sqrt{2}$ is the pion-decay constant. The figure shows that the asymptotic growth that is proportional to μ_q^3 as can be derived in the absence of the mixing is changed into the $m_1^2\mu_q$ dependence due to the mixing. As a result, increment in the density gets milder. It should be noted that the Silver-Blaze property for the quark-number density is obvious since n_q is proportional to Δ.[5]

Before moving on to evaluation of the hadron masses at finite μ_q, we give comments on roles of the spin-1 mean fields $\bar{\omega}$ and $\bar{V}$ in controlling the onset of the baryon superfluid phase. As indicated in Fig. 1, the superfluid phase emerges once μ_q reaches the critical chemical potential (36), which is exactly what lattice simulations suggest [8,17,21]. Note, however, that this is only when we include all the four mean fields: σ_0, Δ, $\bar{\omega}$, and $\bar{V}$. If any of the mean fields were dropped, the critical chemical potential would not coincide with Eq. (36) in the presence of the spin-0 and spin-1 mixing effect. We have checked this property by choosing various parameter sets.[6] In fact, if $\bar{\omega}$ or $\bar{V}$ is neglected while keeping $C = 12$, then the critical chemical potential is found to change to approximately $0.379m_\pi^{(\text{H})}$, which is lower than $\mu_q^{\text{cr}} = m_\pi^{(\text{H})}/2$ suggested by lattice simulations. Accordingly, one can show that the pion mass in the superfluid phase is not given by $m_\pi = 2\mu_q$ that other chiral effective models commonly predict [32,33,36,59]. Furthermore, the Nambu-Goldstone (NG) boson associated with the breakdown of $U(1)_B$ symmetry does not emerge in this case. From these observations, we conclude that $\bar{\omega}$ and $\bar{V}$ as well as σ_0 and Δ play important roles in cold and dense QC_2D matter when the spin-0 and spin-1 mixing effect is present.

V. MASS SPECTRUM

In this section we examine a mass spectrum of the spin-1 hadrons at finite μ_q by expanding the Lagrangian (28) on top of the mean fields obtained in the previous section.

A. General properties

Before showing numerical results for the μ_q dependence of the spin-1 hadron masses, we start with general properties of such hadrons in a medium. In what follows, we consider the rest frame of the medium.

[5]Although the present eLSM predicts $n_q \propto \mu_q$ for larger μ_q, at some point, such a hadronic description would be violated and quark matter would appear, which leads eventually to $n_q \propto \mu_q^3$.

[6]In Sec. VII A, we, indeed, analytically prove that Eq. (36) holds as long as all of σ_0, Δ, $\bar{\omega}$, and $\bar{V}$ are included based on a certain assumption on their critical behaviors.

The quantum numbers carried by (axial-)vector mesons are identical to those of (pseudo)scalar mesons with a derivative, e.g., $a_1^{a,\mu}$ and $\partial^\mu\pi^a$, so that such two kinds of mesons can mix with each other even in the hadronic phase with nonzero C. Similarly, (anti)baryons can mix with the corresponding spin-1 (anti)baryons through a derivative. In the rest frame of the hadronic medium, therefore, the following four mixings appear:

$$(\partial_0\pi, a_1^t), \quad (\partial_0\eta, f_1^t), \quad (\partial_0 B, B_{AS}^t), \quad (\partial_0\bar{B}, \bar{B}_{AS}^t), \quad (40)$$

where each bracket represents the mixing partners and the isospin indices are suppressed for simplicity. Here, the superscript "t" stands for the time component ($\mu = 0$) of the respective spin-1 hadrons. The time components of the spin-1 hadrons are unphysical, so the mixings in Eq. (40) only lead to modifications of π, η, B, and $\bar{B}$, while the physical components, i.e., the spatial components of the spin-1 hadrons remain unaffected. We note that the remaining spin-0 hadrons: σ, a_0, B', and $\bar{B}'$, are not contaminated by any mixing.

Meanwhile, in the baryon superfluid phase the mixings get more complicated due to the $U(1)_B$ baryon-number violation as well as the creation of a baryonic medium. Taking into account the unbroken $SU(2)_I$ isospin symmetry, one can see that the following six mixings are possible:

$$\begin{aligned}
&(\partial_0 a_0, \rho^t),\\
&(\partial_0 B', \partial_0\bar{B}', \partial_0\eta, f_1^t),\\
&(\partial_0\pi, B_S^t, \bar{B}_S^t, a_1^t), \qquad (B_S^s, \bar{B}_S^s, a_1^s)\\
&(\partial_0 B, \partial_0\bar{B}, \partial_0\sigma, B_{AS}^t, \bar{B}_{AS}^t, \omega^t), \qquad (B_{AS}^s, \bar{B}_{AS}^s, \omega^s),
\end{aligned} \quad (41)$$

where each bracket again represents the mixing partners. That is, all of the spin-0 hadronic states are corrected by the corresponding unphysical spin-1 states. Besides, the physical components of B_S, $\bar{B}_S$, a_1, and of B_{AS}, $\bar{B}_{AS}$, ω, are also corrected by the mixings. A schematic picture of the mixings among the hadrons both in the hadronic and superfluid phases are shown in Fig. 3.

In the present paper, the hadron masses are evaluated at tree level in the presence of the mean fields (35). The analysis is straightforward but is complicated and lengthy since, particularly in the superfluid phase, we need to find pole positions of the respective propagator matrix for the mixed states in Eq. (41). For this reason, we leave the detailed procedure to compute the hadron masses to Appendix C.

B. Numerical results for the hadron masses at nonzero μ_q

In this subsection, based on the expressions derived in Appendix C we numerically elucidate μ_q dependence of the

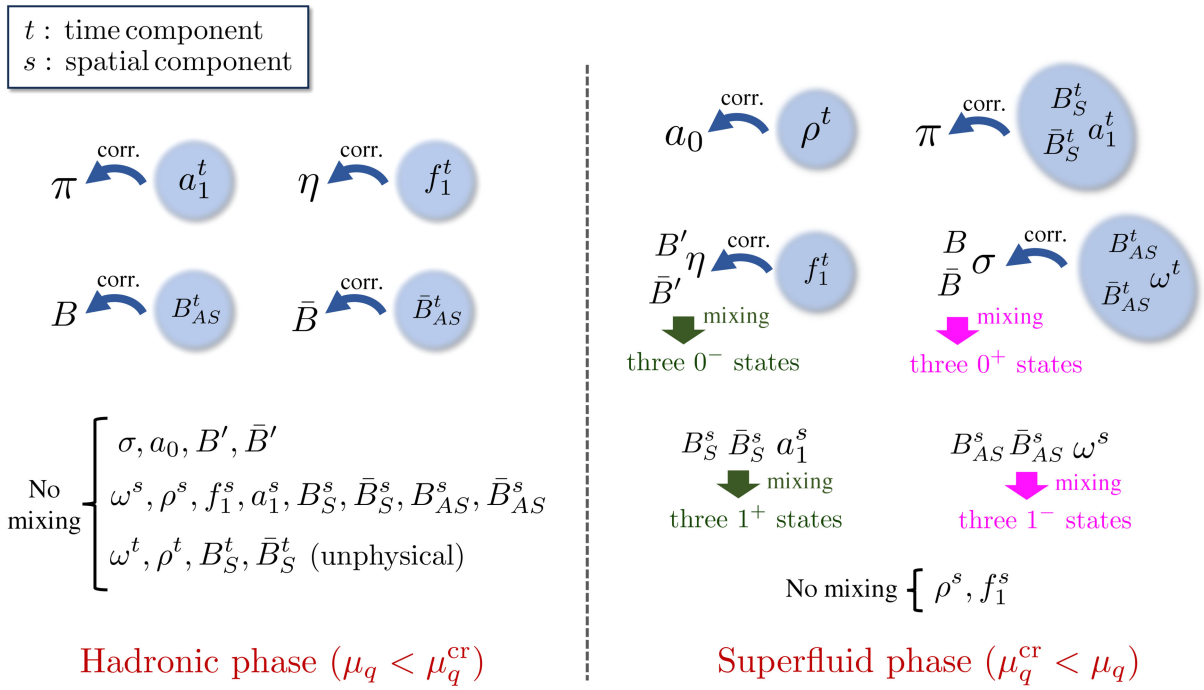

FIG. 3. Schematic picture of corrections to the hadron masses from various mixings.

masses of spin-1 hadrons. As for the free parameters g_Φ and C, we first take $(g_\Phi, C) = (10, 12)$ to draw a typical prediction of the mass spectrum of the spin-1 hadrons. Next, we vary the value of C with g_Φ kept fixed to unveil how the spin-0 and spin-1 mixing affects the mass spectrum. More concretely we take $(g_\Phi, C) = (10, 16)$ and $(g_\Phi, C) = (10, 8)$. Finally, we also choose $(g_\Phi, C) = (5, 12)$ to see influence of the coupling g_Φ on the mass spectrum.

Depicted in Fig. 4 is the resultant μ_q dependence of the spin-1 hadron masses at $(g_\Phi, C) = (10, 12)$. As can be seen from this figure, at vanishing chemical potential, the masses of ω, ρ, B_S, and $\bar{B}_S$ degenerate and so do those of f_1, a_1, B_{AS}, and $\bar{B}_{AS}$. In the hadronic phase, as μ_q increases, all the meson masses do not change and the (anti)baryon masses simply modified linearly. These stable behaviors are reminiscent of the Silver-Blaze property. Here, the slopes of the linear decrement (increment) of diquark (antidiquark) baryons can be understood by their baryon numbers. More explicitly, their mass formulas are given by Eqs. (D3) and (D4). In the baryon superfluid phase, on the other hand, due to the $U(1)_B$ baryon-number violation, ω-B_{AS}-$\bar{B}_{AS}$ mixing and a_1-B_S-$\bar{B}_S$ mixing take place, leading to nonmonotonic μ_q dependence of the masses of the resulting mixed states. Most remarkably, the a_1-B_S-$\bar{B}_S$ mixing has been observed by the recent lattice simulation [62].

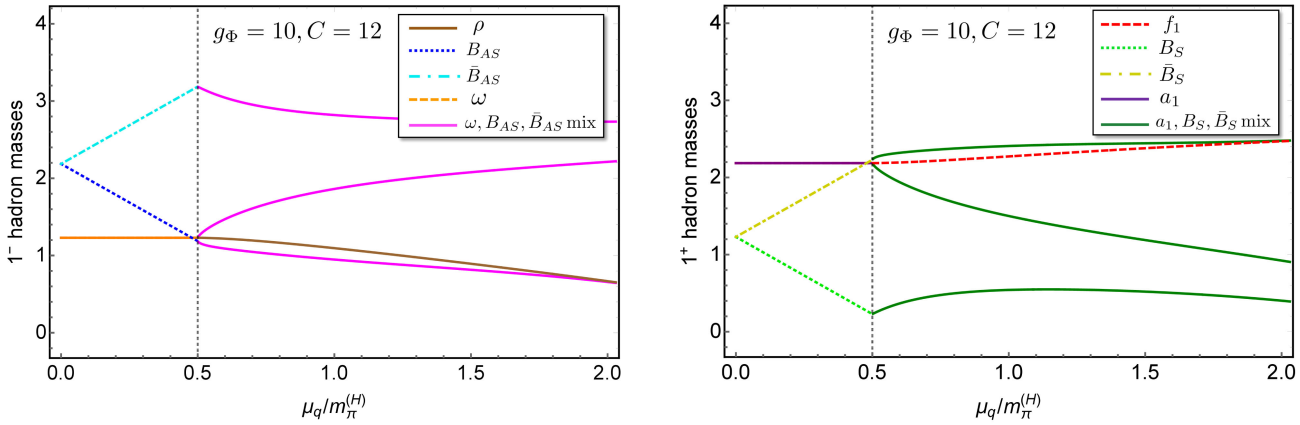

FIG. 4. μ_q dependence of the masses of negative-parity (left) and positive-parity (right) spin-1 hadrons for $(g_\Phi, C) = (10, 12)$. In this figure the masses are normalized by $m_\pi^{(\mathrm{H})}$.

Meanwhile, the ρ and f_1 mesons are not contaminated by any mixing so that those masses depend on μ_q fairly monotonically. We note that the present parameter set yields a slight reduction of the ρ meson mass in the superfluid phase, which is consistent with the lattice data [61,62].

In the presence of the spin-0 and spin-1 mixing effect, it is worth examining the mass spectrum of the spin-0 hadrons in addition to that of the spin-1 hadrons as depicted in Fig. 4. In Fig. 5, we thus draw the resultant μ_q dependence of the spin-0 hadron masses at $(g_\Phi, C) = (10, 12)$. In this figure, the hadron masses are again shown to depend on μ_q monotonically in the hadronic phase, which is consistent with the Silver-Blaze property. Besides, in the superfluid phase, the left panel indicates that a massless mode emerges in the σ-B-$\bar{B}$ mixed state. This mode corresponds to a NG boson associated with the spontaneous breakdown of $U(1)_B$ baryon-number symmetry. Moreover, from the right panel, the pion mass is found to increase linearly in the superfluid phase; this numerical result can be reproduced by a simple formula,

$$m_\pi = 2\mu_q, \tag{42}$$

which is consistent with other chiral models [32,33,36,59]. We again emphasize that all these reasonable results stem from the present correct treatment of the four mean fields (35) within the eLSM.

C. C dependence of the mass spectrum

The mass spectrum of the spin-1 hadrons presented in Fig. 4 is just a typical example. In this case, the value of C is fixed such that the slight reduction of the ρ meson mass in the superfluid phase suggested by lattice simulations is successfully reproduced. Next, we change the value of C while keeping $g_\Phi = 10$. When we take C to be larger, e.g., $C = 16$, the μ_q dependence of the spin-1 hadron masses is obtained as depicted in Fig. 6. From this figure one can find that the mass spectrum in the hadronic phase is identical to the one with $(g_\Phi, C) = (10, 12)$, Fig. 4, as long as all the other parameters are the same. In the superfluid phase, the ρ meson mass slightly increases with μ_q, which is clearly different from the lattice result. This suggests that the

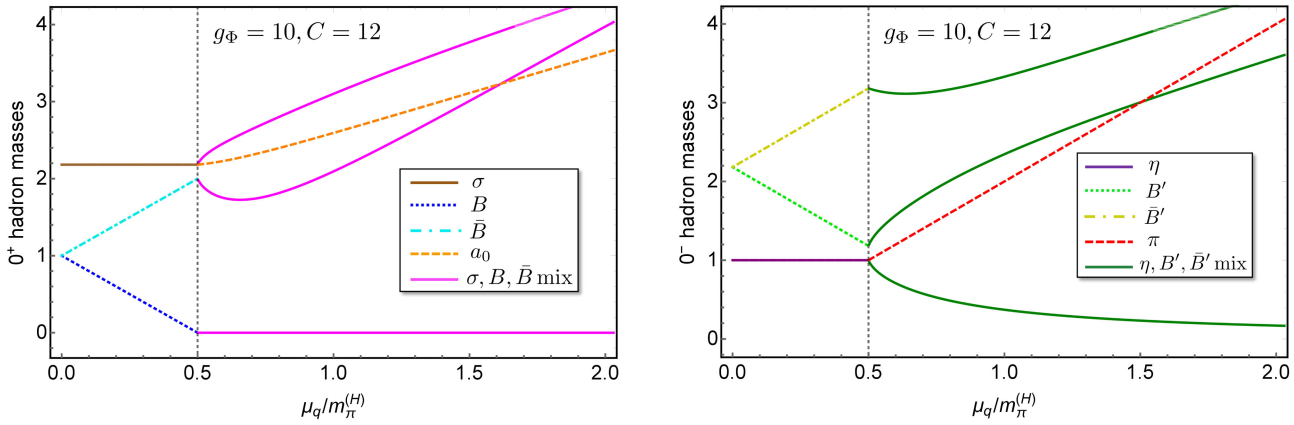

FIG. 5. μ_q dependence of the masses of positive-parity (left) and negative-parity (right) spin-0 hadrons for $(g_\Phi, C) = (10, 12)$. In this figure the masses are normalized by $m_\pi^{(\mathrm{H})}$.

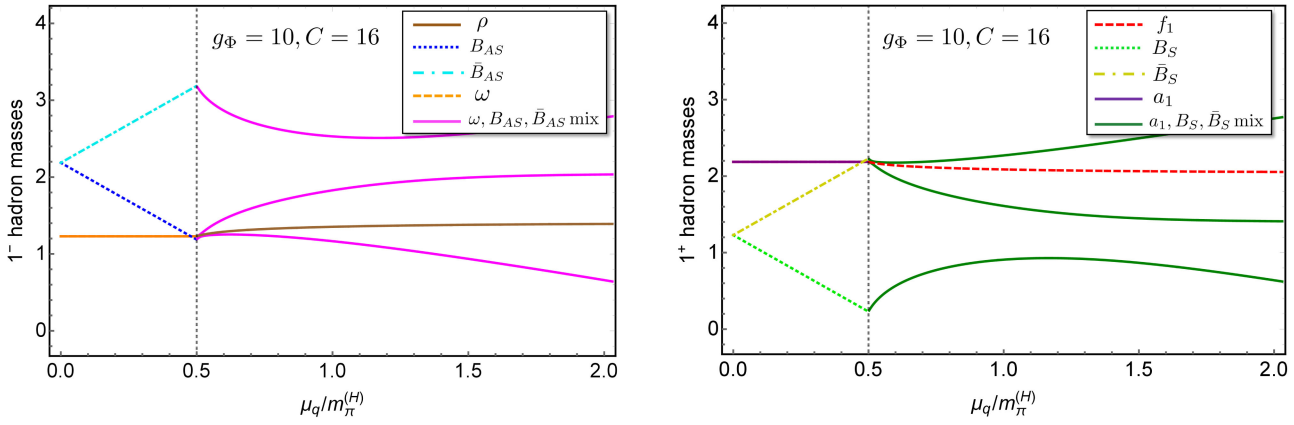

FIG. 6. Same as Fig. 4 but for $(g_\Phi, C) = (10, 16)$.

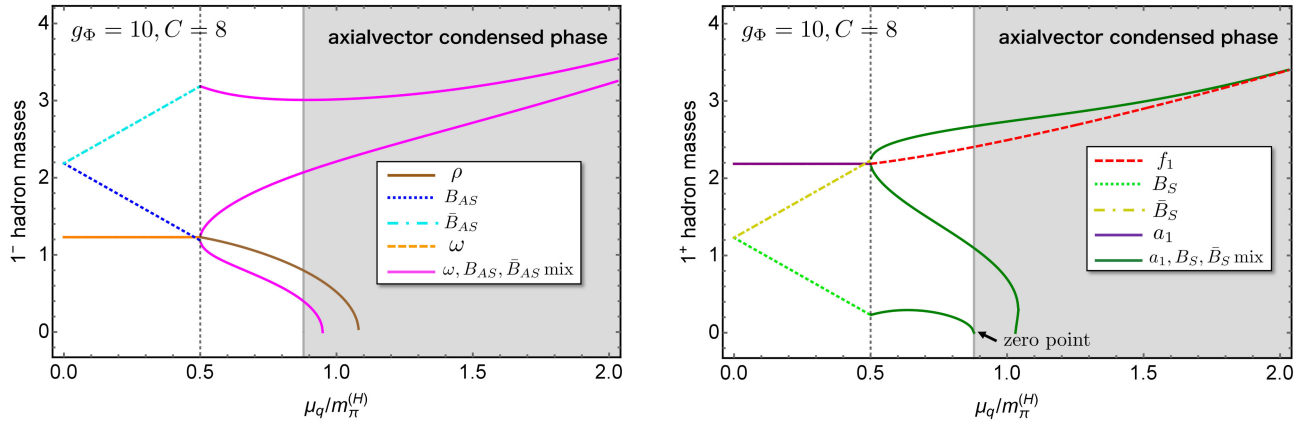

FIG. 7. Same as Fig. 4 but for $(g_\Phi, C) = (10, 8)$.

relevant value of the parameter C that controls the magnitude of the spin-0 and spin-1 mixing effect could not be so large. We note that, since the renormalization factor Z_π (or Z_η), Eq. (D11), must be real, the inputs presented in Sec. III already constrains C as $C \lesssim 18.3$.

When we take C to be smaller, e.g., $C = 8$, the mass spectrum is evaluated as in Fig. 7. The right panel indicates that, in this parameter choice, the mass of the lowest-lying a_1-B_S-$\bar{B}_S$ mixed state reaches zero at $\mu_q \approx 0.88 m_\pi^{(\mathrm{H})}$, as the chemical potential increases in the superfluid phase. Since this mode includes an isotriplet axial-vector component, it is reasonable to argue that above this chemical potential, an axial-vector condensed phase where $SU(2)_I$ isospin symmetry is broken emerges on top of the baryon superfluidity [34], as exhibited by the shaded area in Fig. 7. Thus, the true mass spectrum in this phase is obscure although we have still plotted the numerical result. For a self-consistent analysis, however, it would be necessary to include another mean field that is responsible for the axial-vector condensed phase.

Above the critical chemical potential $\mu_q \approx 0.88 m_\pi^{(\mathrm{H})}$, the mass of the lowest-lying ω-B_{AS}-$\bar{B}_{AS}$ mixed state also converges to zero at $\mu_q \approx 0.95 m_\pi^{(\mathrm{H})}$ as indicated in the left panel of Fig. 7. Besides, the ρ meson mass also becomes zero at $\mu_q \approx 1.1 m_\pi^{(\mathrm{H})}$. These critical chemical potentials lie in the axial-vector condensed phase, so that more precise determination of their values would require extension of the present exploratory analysis. From those findings, however, at least one could expect the existence of the vector condensed phase. We note that the axial-vector condensation occurs prior to the vector condensation, reflecting the fact that the B_S mass is invariably lighter than the B_{AS} one at $\mu_q = \mu_q^{\mathrm{cr}}$, since B_S is an S-wave state.

From the above analysis, one can infer that when C is small enough, the appearance of the axial-vector (and vector) condensate in the superfluid phase is favored. To see this tendency more clearly, in Fig. 8, we plot the critical chemical potential for the appearance of the axial-vector condensed phase as a function of the mixing strength C. In this figure, the pure baryon superfluid phase lies below the curve, while in the above shaded area the axial-vector condensate emerges in the superfluid phase. The figure indeed indicates that the smaller value of C triggers the axial-vector condensation at lower μ_q. In other words, the spin-0 and spin-1 mixing controlled by C acts as a stabilizer to avoid emergence of the axial-vector condensate, i.e., onset of the Bose-Einstein condensation of parity-even spin-1 hadrons, in the low density regime. We note that, even when we take a value of C as large as possible, we find the critical chemical potential for the axial-vector condensation at a certain value, which could be too high for the present model to be valid.

D. g_Φ dependence of the mass spectrum

Thus far we have only varied the value of C, while keeping $g_\Phi = 10$, to focus on the spin-0 and spin-1 mixing effects on the hadron mass spectrum. Let us now examine effects of the coupling g_Φ. When we employ $(g_\Phi, C) = (5, 12)$, the mass spectrum is obtained as in Fig. 9. This figure exhibits appearance of the axial-vector

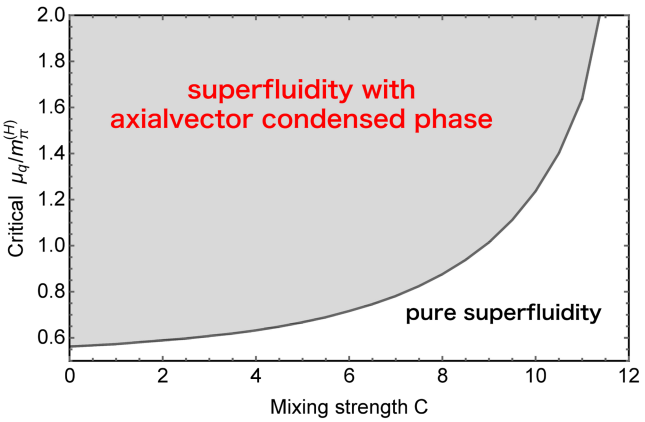

FIG. 8. Critical chemical potential for the axial-vector condensation as a function of mixing strength C. We take $g_\Phi = 10$.

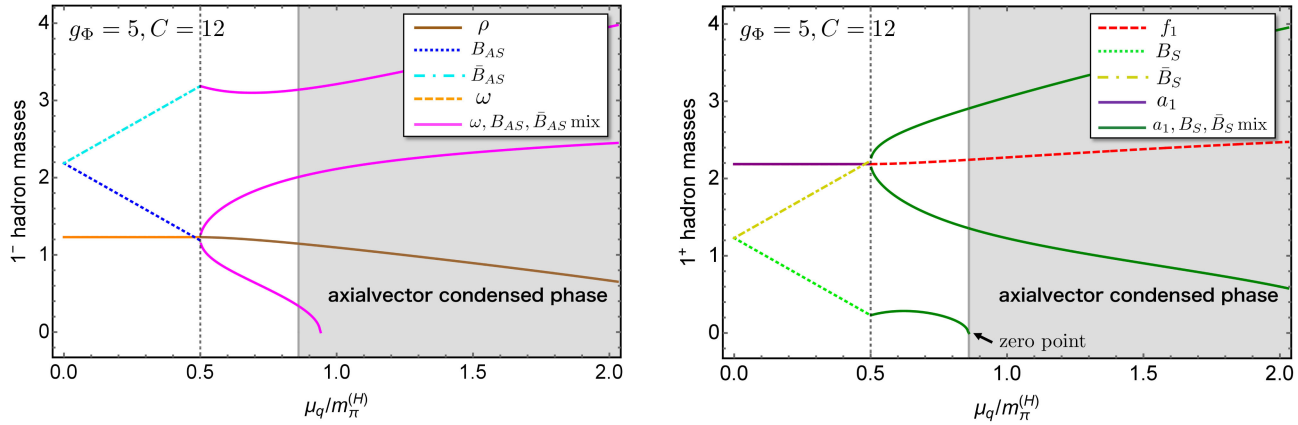

FIG. 9. Same as Fig. 4 but for $(g_\Phi, C) = (5, 12)$.

condensate and possibly of the vector condensate similarly to Fig. 7. One obvious distinction is the qualitative behavior of the ρ meson mass. The μ_q dependence of the ρ meson mass in Fig. 9 does not change from that in Fig. 4 in the sense that both show the same gradual decrease with μ_q, whereas the ρ meson mass in Fig. 7 decreases rapidly to zero. This characteristic behavior can be understood by the fact that the ρ meson mass has no dependence on g_Φ, as shown in Eq. (C6). Thus, g_Φ plays a role in changing the μ_q dependence of the ω-B_{AS}-$\bar{B}_{AS}$ mixed states and the a_1-B_S-$\bar{B}_S$ mixed states, particularly the lowest one for each. Detailed consideration of th ρ meson mass in the superfluid phase will be done in Sec. VII B.

Depicted in Fig. 10 is the g_Φ dependence of the critical chemical potential for the axial-vector condensation. In this figure the axial-vector condensed phase is indicated by the shaded area. Figure 10 implies that the smaller value of g_Φ leads to the appearance of the axial-vector condensate at lower μ_q. Moreover, one can see that reentrant axial-vector condensation occurs in a regime of large g_Φ in such a way that the intervening pure superfluid region shrinks with increasing μ_q.

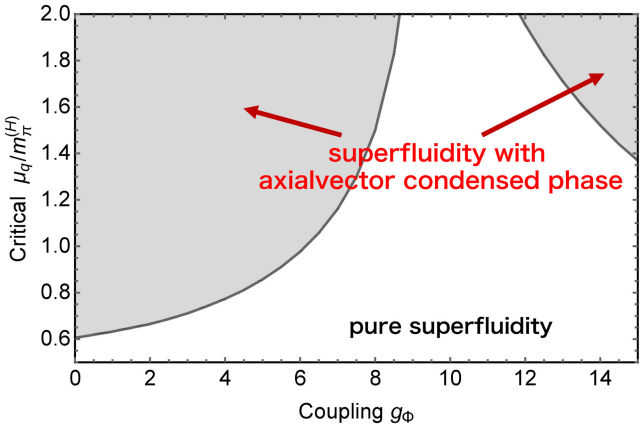

FIG. 10. Critical chemical potential for the axial-vector condensation as a function of the coupling g_Φ. We take $C = 12$.

E. Signs of C and g_Φ

We conclude this section by giving comments on the signs of C and g_Φ. Throughout the above numerical analysis, we have assumed $C > 0$ and $g_\Phi > 0$. When the signs are taken to be $C < 0$ and $g_\Phi < 0$, we can obtain qualitatively similar results for the mass spectrum although the detailed numerical values are slightly changed. For instance, a negatively larger value of C acts to prevent the axial-vector condensation and possible vector condensation from occurring in the superfluid phase. On the other hand, when we take $C > 0$ and $g_\Phi < 0$ or $C < 0$ and $g_\Phi > 0$, the resultant mass spectrum always exhibits both types of condensation in the range of $m_\pi^{(\mathrm{H})}/2 < \mu_q \lesssim 2m_\pi^{(\mathrm{H})}$.

VI. CHIRAL PARTNER STRUCTURE

From the numerical analysis in Sec. V, we have succeeded in gaining insights into roles of the mixing strength C and the coupling g_Φ in determining the spin-1 hadron masses at finite μ_q. In this section, by focusing on a high μ_q regime where chiral symmetry is sufficiently restored, we demonstrate the so-called chiral partner structure of the spin-1 hadrons by identifying the pairs of 1^+ and 1^- hadrons that are degenerate in mass.

At sufficiently high μ_q, the four mean fields would asymptotically behave as $\sigma_0 \to \sigma_\infty \mu_q^{-2}$, $\Delta \to \Delta_\infty$, $\bar{\omega} \to \bar{\omega}_\infty \mu_q$, and $\bar{V} \to \bar{V}_\infty \mu_q^{-1}$, as expected from the numerical results in Fig. 1, where σ_∞, Δ_∞, $\bar{\omega}_\infty$, and $\bar{V}_\infty$ are constants. Using these asymptotic behaviors and the mass formulas derived in Appendix C, first, one can easily show $m_\omega = m_{f_1}$ and $m_\rho = m_{a_1}$ at $\mu_q \to \infty$, where ω and a_1 mesons are decoupled from the respective mixings with the (anti)diquark baryons.[7] That is, (ω, f_1) and (ρ, a_1) can be regarded as the chiral partners even in the presence of the mean fields Δ and $\bar{\omega}$ in a high density region. Next, as for

[7]Here, the superscript "s" for the hadron masses representing the spatial component is omitted for simplicity. The same abbreviation applies to Eq. (54) to refer to the ρ meson mass.

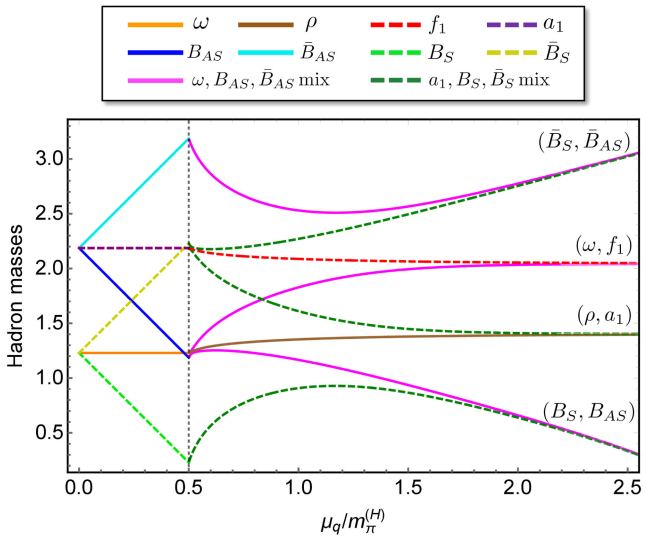

FIG. 11. μ_q dependence of all the 1^+ and 1^- hadron masses for $(g_\Phi, C) = (10, 16)$. The chiral partner structures are clearly shown by the degeneracy.

the remaining (anti)diquark baryons, B_S, $\bar{B}_S$, B_{AS}, and $\bar{B}_{AS}$, the asymptotic behaviors of the mean fields tell that the mixing structures for the V_9-V_{10} system and the V_4'-V_5' system become identical while the remaining bare masses satisfy $m_{V_9} = m_{V_4'}$ and $m_{V_{10}} = m_{V_5'}$ at $\mu_q \to \infty$, as can be seen from Appendix C. Thus, (B_S, B_{AS}) and $(\bar{B}_S, \bar{B}_{AS})$ are also regarded as the chiral partners.

The above analytic consideration of the chiral partner structure is, indeed, numerically confirmed as shown in Fig. 11. In this figure we have taken $(g_\Phi, C) = (10, 16)$ to see the mass degeneracy clearly. Figure 11 indicates that the mass degeneracy occurs between the following 1^+ and 1^- hadrons, (B_S, B_{AS}), (ρ, a_1), (ω, f_1), and $(\bar{B}_S, \bar{B}_{AS})$ from below, at high μ_q. We note that the chiral partner structure for the spin-0 hadrons in the absence of the $U(1)_A$ anomaly was examined in Ref. [59], where mass degeneracy was demonstrated for (B, B'), (σ, π), (a_0, η), and $(\bar{B}, \bar{B}')$.

VII. DISCUSSIONS

A. Analytic derivation of $\mu_q^{\rm cr} = m_\pi^{\rm (H)}/2$ in the eLSM

In Sec. IV, we have numerically seen that the phase transition from the hadronic phase to the baryon superfluid phase takes place just when μ_q coincides with $m_\pi^{\rm (H)}/2$, similarly to other chiral models ignoring spin-1 hadrons [32,33,36,59]. In this section we analytically prove such a universal property within our present eLSM based on a reasonable assumption.

The μ_q dependence of the mean fields, σ_0, Δ, $\bar{\omega}$, and $\bar{V}$, has been determined by stationary conditions in Sec. IV. These conditions can be derived from Eq. (28) as

$$\sigma_0\colon\ \frac{2\sqrt{2}h_q}{\sigma_0} - \frac{C}{\sqrt{2}\sigma_0}\mu_q\Delta\bar{V} - \frac{C_3}{4\sigma_0}\Delta\bar{V}\,\bar{\omega} + \frac{C_3}{8}(\bar{V}^2 - \bar{\omega}^2) + \frac{C}{8}(\bar{V}^2 + \bar{\omega}^2) - m_0^2 - \frac{\lambda_2}{4}(\sigma_0^2 + \Delta^2) = 0, \tag{43}$$

$$\Delta\colon\ -\frac{C}{\sqrt{2}\Delta}\mu_q\bar{V}\sigma_0 - \frac{C_3}{4\Delta}\bar{V}\sigma_0\bar{\omega} + 4\mu_q^2 + \sqrt{2}C\mu_q\bar{\omega} - \frac{C_3}{8}(\bar{V}^2 - \bar{\omega}^2) + \frac{C}{8}(\bar{V}^2 + \bar{\omega}^2) - m_0^2 - \frac{\lambda_2}{4}(\sigma_0^2 + \Delta^2) = 0, \tag{44}$$

$$\bar{\omega}\colon\ \frac{C}{\sqrt{2}\bar{\omega}}\mu_q\Delta^2 - \frac{C_3}{4\bar{\omega}}\Delta\bar{V}\sigma_0 - \frac{C_3}{8}(\sigma_0^2 - \Delta^2) + \frac{C}{8}(\sigma_0^2 + \Delta^2) + m_1^2 = 0, \tag{45}$$

and

$$\bar{V}\colon\ -\frac{C}{\sqrt{2}\bar{V}}\mu_q\Delta\sigma_0 - \frac{C_3}{4\bar{V}}\Delta\sigma_0\bar{\omega} + \frac{C_3}{8}(\sigma_0^2 - \Delta^2) + \frac{C}{8}(\sigma_0^2 + \Delta^2) + m_1^2 = 0. \tag{46}$$

The numerical solutions imply that emergence of $\bar{\omega}$ and $\bar{V}$ is accompanied by nonzero Δ, i.e., by the onset of the baryon superfluidity and that the phase transition is of second order. Let us now suppose that the critical exponents of Δ and $\bar{V}$ are $+1/2$ while that of $\bar{\omega}$ is $+1$. Indeed, these exponents are suggested by the numerical result. Then, Δ and $\bar{V}$ take the form of

$$\begin{aligned}\Delta &\sim \Delta^{\rm cr}(\mu_q - \mu_q^{\rm cr})^{1/2},\\ \bar{V} &\sim \bar{V}^{\rm cr}(\mu_q - \mu_q^{\rm cr})^{1/2},\\ \bar{\omega} &\sim \bar{\omega}^{\rm cr}(\mu_q - \mu_q^{\rm cr})^{1},\end{aligned} \tag{47}$$

in the vicinity of the phase transition, where $\Delta^{\rm cr} > 0$, $\bar{V}^{\rm cr} > 0$, and $\bar{\omega}^{\rm cr} < 0$. From these exponents, one finds that in the limit of $\mu_q \to \mu_q^{\rm cr}$, $\Delta^2/\bar{\omega}$, $\Delta\bar{V}/\bar{\omega}$, and $\Delta/\bar{V}$ approach nonzero values, while $\Delta\bar{\omega}/\bar{V} \to 0$. Thus, the first and second terms of Eq. (45) and the first term in Eq. (46), which remain finite at the critical chemical potential, act as catalyzers to yield nonzero $\bar{\omega}$ and $\bar{V}$ above $\mu_q = \mu_q^{\rm cr}$, respectively.

Given the critical behavior (47), at $\mu_q = \mu_q^{\rm cr}$, the stationary conditions, Eqs. (43)–(46), are reduced to

$$\frac{2\sqrt{2}h_q}{\sigma_0^{\rm (H)}} - Z_\pi^{-2}(m_\pi^{\rm (H)})^2 = 0, \tag{48}$$

$$-\frac{C\mu_q^{\rm cr}\sigma_0^{\rm (H)}}{\sqrt{2}x} + 4(\mu_q^{\rm cr})^2 - Z_\pi^{-2}(m_\pi^{\rm (H)})^2 = 0, \tag{49}$$

$$\frac{C\mu_q^{\rm cr} y}{\sqrt{2}} - \frac{C_3\sigma_0^{(\rm H)} y}{4x} + (m_\rho^{(\rm H)})^2 = 0, \tag{50}$$

and

$$-\frac{C\mu_q^{\rm cr}\sigma_0^{(\rm H)} x}{\sqrt{2}} + (m_{f_1}^{(\rm H)})^2 = 0, \tag{51}$$

respectively, where we have used the hadron mass formulas in Appendix D and defined

$$x \equiv \frac{\Delta^{\rm cr}}{\bar{V}^{\rm cr}} > 0, \qquad y \equiv \frac{(\Delta^{\rm cr})^2}{\bar{\omega}^{\rm cr}} < 0. \tag{52}$$

From Eqs. (49) and (51) as well as the renormalization factor (D11), therefore, one can analytically prove

$$\mu_q^{\rm cr} = \frac{m_\pi^{(\rm H)}}{2}, \tag{53}$$

which was numerically confirmed in Fig. 1. We note that C cannot be zero from the stationary condition for $\bar{V}$ at $\mu_q = \mu_q^{\rm cr}$, Eq. (51), as long as Eq. (47) holds. In other words, $\bar{V}$ always vanishes when $C = 0$, and similarly, from Eq. (50) one can see $\bar{\omega} = 0$ at any μ_q when $C = 0$.

B. Comments on the ρ mass reduction

Here we provide comments on the ρ meson mass reduction in the superfluid phase.

As derived in Eq. (C6), the ρ meson mass is evaluated as

$$m_\rho^2 = m_1^2 + \frac{C - C_3}{8}(\sigma_0^2 + \Delta^2), \tag{54}$$

in both the hadronic and superfluid phases. This universal structure stems from the fact that the ρ meson is not contaminated by any mixing with other hadrons, even in the presence of the superfluidity. Then, if the combination $\sigma_0^2 + \Delta^2$ is enhanced in the superfluid phase while $C < C_3$, the m_ρ reduction observed on the lattice can be reproduced within the present eLSM. From Fig. 2, however, one can see that the enhancement of the combination $\sigma_0^2 + \Delta^2$ in the superfluid phase gets mild as the spin-0 and spin-1 mixing effect becomes prominent. That is why m_ρ is relatively hard to change for a larger value of C.

Since μ_q dependence of the combination $\sigma_0^2 + \Delta^2$ in the superfluid phase is rather monotonic as can be inferred from Fig. 2, the resultant m_ρ also changes almost linearly as a function of μ_q. On the other hand, the lattice data would imply a rather abrupt reduction of m_ρ just above $\mu_q = \mu_q^{\rm cr}$, although there remain error bars; μ_q dependence of m_ρ measured by the lattice simulation would look convex downward [61,62]. One promising mechanism to yield such a downward-convex behavior of m_ρ could be additional mixing with other states that are associated with the superfluidity but have yet to be considered in the present analysis. The ρ meson, which is an isotriplet state carrying $J^P = 1^-$, may strongly mix with an isotriplet and $J^P = 1^-$ diquark $\tilde{B}^i \sim \epsilon^{ijk}[\psi^T C\Sigma^{jk}\tau_c^2\psi]_{\rm sym}$, where $\Sigma^{\mu\nu} = \frac{i}{2}[\gamma^\mu, \gamma^\nu]$ is the antisymmetric tensor and the subscript "sym." means the flavor symmetric structure. Inclusion of this new diquark state, however, requires us to introduce another quark bilinear operator $\tilde{\Phi}_{ij}^{\mu\nu} \sim \Psi_j^T\sigma^2\bar{\sigma}^{\mu\nu}\tau_c^2\Psi_i$, where $\bar{\sigma}^{\mu\nu} = \frac{i}{2}(\bar{\sigma}^\mu\sigma^\nu - \bar{\sigma}^\nu\sigma^\mu)$ with $\bar{\sigma}^\mu = (\mathbf{1}, -\sigma^i)$, which is beyond the scope of the present study. Thus, we leave detailed examination of the $\tilde{B}^i$-ρ mixing in the superfluid phase for future study.

VIII. CONCLUSIONS

In summary, for dense $\mathrm{QC_2D}$ at zero temperature, we have constructed the extended linear sigma model, eLSM, in such a way as to respect the Pauli-Gürsey $SU(4)$ symmetry and to describe both the spin-0 and spin-1 hadrons. Then, based on the eLSM, richness of the mass spectrum of the spin-1 hadrons in dense $\mathrm{QC_2D}$ has been explored.

In the baryon superfluid phase where the diquark condensate emerges, we have found that not only the scalar meson and scalar diquark baryon but also the time components of the vector meson and vector diquark baryon possess their mean field values, in the presence of spin-0 and spin-1 mixing. These mean fields are induced by violation of the Lorentz invariance as well as of $U(1)$ baryon-number conservation. Besides, we have analytically shown that the onset condition of superfluidity corresponds to $\mu_q = m_\pi^{(\rm H)}/2$ ($m_\pi^{(\rm H)}$ is the pion mass in the hadronic phase) and that the pion mass in the superfluid phase reads $m_\pi = 2\mu_q$. Moreover, the appearance of the NG boson associated with $U(1)_B$ violation has been confirmed. Those self-consistent properties, which were numerically indicated by lattice simulations, are derived only when the above four types of mean fields are included.

Inclusion of the vector-meson and vector-diquark mean fields has led to suppression of the otherwise substantial increase of the scalar-diquark mean field in the superfluid phase via the spin-0 and spin-1 mixing. Simultaneously, it has been found that the slight reduction of the ρ meson mass in the superfluid phase suggested by the lattice data is successfully reproduced in the presence of the significant spin-0 and spin-1 mixing. Furthermore, by varying the magnitude of this mixing and of coupling among the spin-1 hadrons, we have demonstrated the emergence of the axial-vector condensate and the possible vector condensate. Those novel condensates are induced when the masses of the corresponding modes reach zero. Given such condensates, therefore, it is inevitable to investigate the in-medium masses of the spin-1 hadrons from the first-principles lattice calculation of dense $\mathrm{QC_2D}$ toward further delineation of the phase structures.

In addition, we have also discussed a possible existence of an isotriplet 1^- diquark, motivated by the possible downward-convex behavior of the ρ meson mass reduction in the superfluid phase as suggested by the lattice simulations [61,62]. This diquark is denoted by a tensor-type quark bilinear field, while no examination has been done so far. Therefore, it would be challenging to pursue properties of such a new diquark state from both effective theories and first-principles numerical studies.

ACKNOWLEDGMENTS

The authors thank Masayasu Harada for useful comments on the HLS formalism for the spin-1 hadrons. D. S. was supported by the RIKEN special postdoctoral researcher program and by the Japan Society for the Promotion of Science (JSPS) KAKENHI Grant No. 23K03377. K. M. is supported in part by JST SPRING with Grant No. JPMJSP2110, by Grants-in-Aid for JSPS Fellows (No. JP22J14889 and JP22KJ1870), and by JSPS KAKENHI with Grant No. 22H04917. The work of K. I. is supported by JSPS KAKENHI with Grants No. 18H05406 and No. 23H01167. The work of E. I. is supported by JSPS KAKENHI with Grant No. 23H05439, JST PRESTO Grant No. JPMJPR2113, JSPS Grant-in-Aid for Transformative Research Areas (A) JP21H05190, JST Grant No. JPMJPF2221 and also supported by Program for Promoting Researches on the Supercomputer "Fugaku" (Simulation for basic science: from fundamental laws of particles to creation of nuclei) and (Simulation for basic science: approaching the new quantum era), and Joint Institute for Computational Fundamental Science (JICFuS), Grant No. JPMXP1020230411. The work of E. I. is supported also by Center for Gravitational Physics and Quantum Information (CGPQI) at YITP.

APPENDIX A: THE PAULI-GÜRSEY $SU(4)$ SYMMETRY IN TWO-FLAVOR QC_2D

In this appendix, we briefly show emergence of the Pauli-Gürsey $SU(4)$ symmetry in QC_2D with two flavors [32,33].

The QC_2D Lagrangian for massless u and d quarks is of the form,

$$\mathcal{L}_{QC_2D} = \bar{\psi} i \not{D} \psi, \tag{A1}$$

where $\psi = (u, d)^T$ is the quark doublet and $D_\mu \psi = \partial_\mu \psi - i g_c A_\mu^a T_c^a \psi$ is the covariant derivative describing interactions between the quarks ψ and gluons A_μ^a. The 2×2 matrix $T_c^a = \tau_c^a/2$ is the $SU(2)_c$ generator ($\boldsymbol{\tau_c^a}$ is the Pauli matrix for colors). Adopting the Weyl representation for the Dirac matrices, the Lagrangian (A1) can be expressed in terms of left-handed and right-handed quarks as

$$\begin{aligned}\mathcal{L}_{QC_2D} = {} & \psi_R^\dagger i \partial_\mu \sigma^\mu \psi_R - g_c \psi_R^\dagger A_\mu^a T_c^a \sigma^\mu \psi_R \\ & + \psi_L^\dagger i \partial_\mu \bar{\sigma}^\mu \psi_L - g_c \psi_L^\dagger A_\mu^a T_c^a \bar{\sigma}^\mu \psi_L. \end{aligned} \tag{A2}$$

In this Lagrangian, $u = (u_R, u_L)^T$ and $d = (d_R, d_L)^T$ in the Weyl representation, and the 2×2 matrices in the spinor space are defined by $\sigma^\mu = (\mathbf{1}, \sigma^i)$ and $\bar{\sigma}^\mu = (\mathbf{1}, -\sigma^i)$ with the Pauli matrix σ^i. Here, we make use of the pseudoreal property of the Pauli matrix. Namely, using relations

$$T_c^a = -\tau_c^2 (T_c^a)^T \tau_c^2, \qquad \sigma^i = -\sigma^2 (\sigma^i)^T \sigma^2, \tag{A3}$$

and accordingly introducing the "conjugate quark fields"

$$\tilde{\psi}_R \equiv \sigma^2 \tau_c^2 \psi_R^*, \qquad \tilde{\psi}_L \equiv \sigma^2 \tau_c^2 \psi_L^*, \tag{A4}$$

the Lagrangian (A2) can be expressed in a unified form as

$$\mathcal{L}_{QC_2D} = \Psi^\dagger i \partial_\mu \sigma^\mu \Psi - g \Psi^\dagger A_\mu^a \sigma^\mu \Psi. \tag{A5}$$

Here, we have described the quark fields by using a four-component column vector defined as

$$\Psi \equiv \begin{pmatrix} \psi_R \\ \tilde{\psi}_L \end{pmatrix} = \begin{pmatrix} u_R \\ d_R \\ \tilde{u}_L \\ \tilde{d}_L \end{pmatrix}. \tag{A6}$$

The Lagrangian (A5) is obviously invariant under an $SU(4)$ transformation of

$$\Psi \to U \Psi \quad \text{with} \quad U \in SU(4), \tag{A7}$$

rather than $SU(2)_L \times SU(2)_R$ chiral transformation. Such an extended symmetry is sometimes referred to as the Pauli-Gürsey $SU(4)$ symmetry [32,33]. As can be seen from Eq. (A6), the Pauli-Gürsey $SU(4)$ symmetry is realized by treating ψ and $\tilde{\psi}$ in a single multiplet, reflecting the fact that mesons and diquark baryons can be described in a unified way in two-flavor QC_2D. It should be noted that the $U(1)_B$ baryon-number transformation is generated by

$$\Psi \to \mathrm{e}^{-i\theta_q J} \Psi \quad \text{with} \quad J \equiv \begin{pmatrix} \mathbf{1} & 0 \\ 0 & -\mathbf{1} \end{pmatrix}, \tag{A8}$$

where $\mathrm{e}^{-i\theta_q J}$ belongs to a subgroup of the Pauli-Gürsey $SU(4)$ group.

APPENDIX B: GENERATORS OF $U(4)$ LIE ALGEBRA

In this appendix, we list the generators of $U(4)$ Lie algebra.

The number of the $U(4)$ generators is $4 \times 4 = 16$. It is convenient to separate these 16 generators into two sets S^i ($i = 1$–10) and X^a ($a = 0$–5) that satisfy,

$$E(S^i)^T = -S^i E, \qquad E(X^a)^T = X^a E, \tag{B1}$$

with the symplectic matrix,

$$E = \begin{pmatrix} 0 & \mathbf{1}_f \\ -\mathbf{1}_f & 0 \end{pmatrix}. \tag{B2}$$

That is, the elements generated by S^i, $h = \mathrm{e}^{-i\theta_S^i S^i}$, exhibit the following relation:

$$hEh^T = E. \tag{B3}$$

This relation means that h belongs to the $Sp(4)$ group, which is the subgroup of the original $U(4)$ group.

More concretely, the generators S^i belonging to the Lie algebra of $Sp(4)$ read

$$S^{i=1-4} = \frac{1}{2\sqrt{2}} \begin{pmatrix} \tau_f^i & 0 \\ 0 & -(\tau_f^i)^T \end{pmatrix},$$
$$S^{i=5-10} = \frac{1}{2\sqrt{2}} \begin{pmatrix} 0 & B^i \\ (B^i)^\dagger & 0 \end{pmatrix}, \tag{B4}$$

with $\tau_f^4 = \mathbf{1}_f$, $B^5 = \mathbf{1}_f$, $B^6 = i\mathbf{1}_f$, $B^7 = \tau_f^3$, $B^8 = i\tau_f^3$, $B^9 = \tau_f^1$, and $B^{10} = i\tau_f^1$. Meanwhile, the remaining generators belonging to the algebras of $U(1)$ and $SU(4)/Sp(4)$ are given by

$$X^{a=0-3} = \frac{1}{2\sqrt{2}} \begin{pmatrix} \tau_f^a & 0 \\ 0 & (\tau_f^a)^T \end{pmatrix},$$
$$X^{a=4,5} = \frac{1}{2\sqrt{2}} \begin{pmatrix} 0 & D^a \\ (D^a)^\dagger & 0 \end{pmatrix}, \tag{B5}$$

where $\tau_f^{a=0} = \mathbf{1}_f$ is the 2×2 unit matrix and $\tau_f^{a=1-3}$ are the Pauli matrices in the flavor space. Besides, $D^4 = \tau_f^2$ and $D^5 = i\tau_f^2$.

APPENDIX C: MASS FORMULAS

In this appendix, we derive hadron mass formulas from the reduced eLSM Lagrangian (28).

The mass formulas are derived by picking up quadratic terms of the hadron fields in the Lagrangian (28) on top of the mean fields σ_0, Δ, $\bar{\omega}$, and $\bar{V}$ defined by Eq. (35). The eLSM describes the mass spectrum of 16 hadrons in total, namely, eight spin-0 hadrons, η, π, B, $\bar{B}$, σ, a_0, B', and $\bar{B}'$, and eight spin-1 hadrons, ω, ρ, B_S, $\bar{B}_S$, f_1, a_1, B_{AS}, and $\bar{B}_{AS}$. As explained in Sec. V A, those 16 hadrons are separated into the following four systems due to different mixing patterns:

(1) a_0-ρ system;
(2) η-B'-$\bar{B}'$-f_1 system;
(3) π-a_1-B_S-$\bar{B}_S$ system;
(4) σ-B-$\bar{B}$-ω-B_{AS}-$\bar{B}_{AS}$ system.

Then, in what follows we show the mass formulas for these four systems separately.

1. a_0-ρ system

As for the a_0-ρ system, the relevant Lagrangian is obtained as

$$\mathcal{L}_{(1)} = \mathcal{L}_{a_0} + \mathcal{L}_\rho + \mathcal{L}_{a_0\rho}, \tag{C1}$$

where each term reads

$$\mathcal{L}_{a_0} = \frac{1}{2}\partial_\mu a_0 \partial^\mu a_0 - \frac{m_{a_0}^2}{2} a_0^2, \tag{C2}$$

$$\mathcal{L}_\rho = -\frac{1}{4}(\partial_\mu \rho_\nu - \partial_\nu \rho_\mu)^2 + \frac{(m_\rho^t)^2}{2}(\rho^0)^2 + \frac{(m_\rho^s)^2}{2}\rho_i \rho^i, \tag{C3}$$

and

$$\mathcal{L}_{a_0\rho} = \frac{C - C_3}{4}(\Delta \bar{V}_4 + \sigma_0 \bar{\omega}) a_0 \rho^0. \tag{C4}$$

In these terms, we have suppressed the isospin indices for simplicity, and have defined the mass parameters by

$$m_{a_0}^2 = m_0^2 + \frac{3\lambda_2}{4}(\sigma_0^2 + \Delta^2) - \frac{C - C_3}{8}(\bar{V}^2 + \bar{\omega}^2), \tag{C5}$$

and

$$(m_\rho^t)^2 = (m_\rho^s)^2 = m_1^2 + \frac{C - C_3}{8}(\sigma_0^2 + \Delta^2), \tag{C6}$$

where the superscripts "t" and "s" are attached to distinguish between time-component (unphysical) and spatial-component (physical) masses.

Thus, from Eq. (C4) one can see that the a_0 meson mixes with the time component of the ρ meson due to the violation of the Lorentz invariance. For this reason, the mass of the a_0 meson does not coincide with m_{a_0} provided by Eq. (C5) but is determined by a pole of the propagator matrix for the a_0-ρ^0 system at vanishing momentum $\boldsymbol{p} = \mathbf{0}$. The inverse of the propagator matrix $i\mathcal{D}_{(1)}^{-1}(p_0, \mathbf{0})$ can be derived as

$$i\mathcal{D}_{(1)}^{-1}(p_0, \mathbf{0}) = \begin{pmatrix} \mathcal{M}_{a_0 a_0} & \mathcal{M}_{a_0\rho} \\ \mathcal{M}_{\rho a_0} & \mathcal{M}_{\rho\rho} \end{pmatrix}, \tag{C7}$$

with

$$\mathcal{M}_{a_0 a_0} = p_0^2 - m_{a_0}^2, \tag{C8}$$

$$\mathcal{M}_{a_0\rho} = \mathcal{M}_{\rho a_0} = \frac{C - C_3}{4}(\Delta \bar{V} + \sigma_0 \bar{\omega}), \tag{C9}$$

and

$$\mathcal{M}_{\rho\rho} = (m_\rho^t)^2. \tag{C10}$$

Therefore, the mass of a_0 at arbitrary μ_q is evaluated by numerically solving $\det[i\mathcal{D}^{-1}_{(1)}(p_0, \mathbf{0})] = 0$. Meanwhile, the spatial components of the ρ meson, i.e., the physical states of ρ do not join any mixing, and hence, the ρ meson mass is identical to m_ρ^s, Eq. (C6).

2. η-B'-$\bar{B}'$-f_1 system

Employing a similar procedure demonstrated in Appendix C 1, the mass spectrum of the η-B'-$\bar{B}'$-f_1 system can be evaluated. In this case, η, B', $\bar{B}'$ (or B'^4, B'^5) and the time component of f_1 can mix. The inverse propagator of these four states at vanishing momentum $\boldsymbol{p} = \mathbf{0}$: $i\mathcal{D}^{-1}_{(2)}(p_0, \mathbf{0})$, is given by

$$i\mathcal{D}^{-1}_{(2)}(p_0, \mathbf{0}) = \begin{pmatrix} \mathcal{M}_{\eta\eta} & \mathcal{M}_{\eta B'_4} & \mathcal{M}_{\eta B'_5} & \mathcal{M}_{\eta f_1} \\ \mathcal{M}_{B'_4\eta} & \mathcal{M}_{B'_4B'_4} & \mathcal{M}_{B'_4B'_5} & \mathcal{M}_{B'_4 f_1} \\ \mathcal{M}_{B'_5\eta} & \mathcal{M}_{B'_5B'_4} & \mathcal{M}_{B'_5B'_5} & \mathcal{M}_{B'_5 f_1} \\ \mathcal{M}_{f_1\eta} & \mathcal{M}_{f_1B'_4} & \mathcal{M}_{f_1B'_5} & \mathcal{M}_{f_1 f_1} \end{pmatrix}, \tag{C11}$$

where each matrix element reads

$$\mathcal{M}_{\eta\eta} = p_0^2 - m_\eta^2 + \frac{C^2}{8}\bar{V}^2, \tag{C12}$$

$$\mathcal{M}_{\eta B'_4} = -\mathcal{M}_{B'_4\eta} = -i\frac{C}{\sqrt{2}}\bar{V}p_0, \tag{C13}$$

$$\mathcal{M}_{\eta B'_5} = \mathcal{M}_{B'_5\eta} = -\frac{2\lambda_2}{4}\sigma_0\Delta + \frac{C}{\sqrt{2}}\bar{V}\mu_q + \frac{C_3}{4}\bar{V}\bar{\omega}, \tag{C14}$$

$$\mathcal{M}_{\eta f_1} = -\mathcal{M}_{f_1\eta} = -i\frac{C}{2\sqrt{2}}\sigma_0 p_0, \tag{C15}$$

$$\mathcal{M}_{B'_4B'_4} = p_0^2 - m_{B'_4}^2 + \frac{C^2}{8}\bar{V}^2 + \left(2\mu_q + \frac{C}{2\sqrt{2}}\bar{\omega}\right)^2, \tag{C16}$$

$$\mathcal{M}_{B'_4B'_5} = -\mathcal{M}_{B'_5B'_4} = 2i\left(2\mu_q + \frac{C}{2\sqrt{2}}\bar{\omega}\right)p_0, \tag{C17}$$

$$\mathcal{M}_{B'_4 f_1} = \mathcal{M}_{f_1B'_4} = \frac{C+C_3}{4}(\sigma_0\bar{V} - \Delta\bar{\omega}) - \sqrt{2}C\Delta\mu_q, \tag{C18}$$

$$\mathcal{M}_{B'_5B'_5} = p_0^2 - m_{B'_5}^2 + \left(2\mu_q + \frac{C}{2\sqrt{2}}\bar{\omega}\right)^2, \tag{C19}$$

$$\mathcal{M}_{B'_5 f_1} = -\mathcal{M}_{f_1B'_5} = i\frac{C}{2\sqrt{2}}\Delta p_0, \tag{C20}$$

and

$$\mathcal{M}_{f_1f_1} = (m_{f_1}^t)^2, \tag{C21}$$

with the mass parameters,

$$m_{B'_4}^2 = m_0^2 + \frac{3\lambda_2}{4}(\sigma_0^2 + \Delta^2) - \frac{C - C^2 + C_3}{8}(\bar{V}^2 + \bar{\omega}^2), \tag{C22}$$

$$m_{B'_5}^2 = m_0^2 + \frac{\lambda_2}{4}(3\sigma_0^2 + \Delta^2) - \frac{C - C^2 + C_3}{8}\bar{\omega}^2 - \frac{C - C_3}{8}\bar{V}^2, \tag{C23}$$

$$m_\eta^2 = m_0^2 + \frac{\lambda_2}{4}(\sigma_0^2 + 3\Delta^2) - \frac{C - C_3}{8}\bar{\omega}^2 - \frac{C - C^2 + C_3}{8}\bar{V}^2, \tag{C24}$$

and

$$(m_{f_1}^t)^2 = m_1^2 + \frac{C}{4}(\sigma_0^2 + \Delta^2). \tag{C25}$$

In the presence of the mixing, the mass spectrum of the η-B'-$\bar{B}'$ system is evaluated by numerically solving $\det[i\mathcal{D}^{-1}_{(2)}(p_0, \mathbf{0})] = 0$. Meanwhile, the space components of f_1 are decoupled, which allows us to simply obtain the physical f_1 meson mass as

$$(m_{f_1}^s)^2 = m_1^2 + \frac{C + C_3}{8}(\sigma_0^2 + \Delta^2). \tag{C26}$$

3. π-a_1-B_S-$\bar{B}_S$ system

Here, we derive the mass formulas for the π-a_1-B_S-$\bar{B}_S$ system. In this case, π and the time components of a_1, B_S, $\bar{B}_S$ (or V^9, V^{10}) can mix. In addition, the space components of a_1, B_S, $\bar{B}_S$ (or V^9, V^{10}) also mix with each other.

First, we consider the mixing among π and the time components of a_1, B_S, and $\bar{B}_S$. The inverse propagator of these four states at vanishing momentum $\boldsymbol{p} = \mathbf{0}$, $i\mathcal{D}^{-1}_{(3)}(p_0, \mathbf{0})$, is given by

$$i\mathcal{D}^{-1}_{(3)}(p_0, \mathbf{0}) = \begin{pmatrix} \mathcal{M}_{\pi\pi} & \mathcal{M}_{\pi a_1} & \mathcal{M}_{\pi V_9} & \mathcal{M}_{\pi V_{10}} \\ \mathcal{M}_{a_1\pi} & \mathcal{M}_{a_1a_1} & 0 & \mathcal{M}_{a_1 V_{10}} \\ \mathcal{M}_{V_9\pi} & 0 & \mathcal{M}_{V_9V_9} & 0 \\ \mathcal{M}_{V_{10}\pi} & \mathcal{M}_{V_{10}a_1} & 0 & \mathcal{M}_{V_{10}V_{10}} \end{pmatrix}, \tag{C27}$$

where each matrix element reads

$$\mathcal{M}_{\pi\pi} = p_0^2 - m_\pi^2, \tag{C28}$$

$$\mathcal{M}_{\pi a_1} = -\mathcal{M}_{a_1\pi} = -i\frac{C}{2\sqrt{2}}\sigma_0 p_0, \tag{C29}$$

$$\mathcal{M}_{\pi V_9} = \mathcal{M}_{V_9\pi} = \frac{C_3}{4}\sigma_0\bar{V} - \frac{C}{\sqrt{2}}\Delta\mu_q - \frac{C_3}{4}\Delta\bar{\omega}, \tag{C30}$$

$$\mathcal{M}_{\pi V_{10}} = -\mathcal{M}_{V_{10}\pi} = i\frac{C}{2\sqrt{2}}\Delta p_0, \tag{C31}$$

$$\mathcal{M}_{a_1 a_1} = (m_{a_1}^t)^2, \tag{C32}$$

$$\mathcal{M}_{a_1 V_{10}} = \mathcal{M}_{V_{10} a_1} = -\frac{C_3}{4}\sigma_0\Delta, \tag{C33}$$

$$\mathcal{M}_{V_9 V_9} = (m_{V_9}^t)^2, \tag{C34}$$

and

$$\mathcal{M}_{V_{10}V_{10}} = (m_{V_{10}}^t)^2, \tag{C35}$$

with the mass parameters

$$m_\pi^2 = m_0^2 + \frac{\lambda_2}{4}(\sigma_0^2 + \Delta^2) - \frac{C - C_3}{8}(\bar{V}^2 + \bar{\omega}^2), \tag{C36}$$

$$(m_{a_1}^t)^2 = m_1^2 + \frac{C}{8}(\sigma_0^2 + \Delta^2) + \frac{C_3}{8}(\sigma_0^2 - \Delta^2), \tag{C37}$$

$$(m_{V_9}^t)^2 = m_1^2 + \frac{C - C_3}{8}(\sigma_0^2 + \Delta^2), \tag{C38}$$

and

$$(m_{V_{10}}^t)^2 = m_1^2 + \frac{C}{8}(\sigma_0^2 + \Delta^2) - \frac{C_3}{8}(\sigma_0^2 - \Delta^2). \tag{C39}$$

In the presence of the mixing, the pion mass is evaluated by numerically solving $\det[i\mathcal{D}_{(3)}^{-1}(p_0, \mathbf{0})] = 0$.

Next, we consider the mixing among the spatial components of a_1, B_S, and $\bar{B}_S$. In this case, the corresponding inverse propagator at vanishing momentum $\boldsymbol{p} = \mathbf{0}$, $i\tilde{\mathcal{D}}_{(3)}^{-1}(p_0, \mathbf{0})$, is given by

$$i\tilde{\mathcal{D}}_{(3)}^{-1}(p_0, \mathbf{0}) = \begin{pmatrix} \tilde{\mathcal{M}}_{a_1 a_1} & \tilde{\mathcal{M}}_{a_1 V_9} & \tilde{\mathcal{M}}_{a_1 V_{10}} \\ \tilde{\mathcal{M}}_{V_9 a_1} & \tilde{\mathcal{M}}_{V_9 V_9} & \tilde{\mathcal{M}}_{V_9 V_{10}} \\ \tilde{\mathcal{M}}_{V_{10} a_1} & \tilde{\mathcal{M}}_{V_{10} V_9} & \tilde{\mathcal{M}}_{V_{10} V_{10}} \end{pmatrix}, \tag{C40}$$

where each matrix element reads

$$\tilde{\mathcal{M}}_{a_1 a_1} = -p_0^2 - \frac{g_\Phi^2}{2}\bar{V}^2 + (m_{a_1}^s)^2, \tag{C41}$$

$$\tilde{\mathcal{M}}_{a_1 V_9} = -\tilde{\mathcal{M}}_{V_9 a_1} = \sqrt{2} i g_\Phi \bar{V} p_0, \tag{C42}$$

$$\tilde{\mathcal{M}}_{a_1 V_{10}} = \tilde{\mathcal{M}}_{V_{10} a_1} = -\frac{C_3}{4}\sigma_0\Delta - \sqrt{2} g_\Phi \bar{V}\mu_q - \frac{g_\Phi^2}{2}\bar{V}\,\bar{\omega}, \tag{C43}$$

$$\tilde{\mathcal{M}}_{V_9 V_9} = -p_0^2 - \frac{g_\Phi^2}{2}\bar{V}^2 - \left(2\mu_q + \frac{g_\Phi}{\sqrt{2}}\bar{\omega}\right)^2 + (m_{V_9}^s)^2, \tag{C44}$$

$$\tilde{\mathcal{M}}_{V_9 V_{10}} = -\tilde{\mathcal{M}}_{V_{10} V_9} = -2i\left(2\mu_q + \frac{g_\Phi}{\sqrt{2}}\bar{\omega}\right)p_0, \tag{C45}$$

and

$$\tilde{\mathcal{M}}_{V_{10} V_{10}} = -p_0^2 - \left(2\mu_q + \frac{g_\Phi}{\sqrt{2}}\bar{\omega}\right)^2 + (m_{V_{10}}^s)^2, \tag{C46}$$

with the mass parameters

$$(m_{a_1}^s)^2 = m_1^2 + \frac{C}{8}(\sigma_0^2 + \Delta^2) + \frac{C_3}{8}(\sigma_0^2 - \Delta^2), \tag{C47}$$

$$(m_{V_9}^s)^2 = m_1^2 + \frac{C - C_3}{8}(\sigma_0^2 + \Delta^2), \tag{C48}$$

and

$$(m_{V_{10}}^s)^2 = m_1^2 + \frac{C}{8}(\sigma_0^2 + \Delta^2) - \frac{C_3}{8}(\sigma_0^2 - \Delta^2). \tag{C49}$$

In the presence of the mixing, the mass spectrum for the a_1-B_S-$\bar{B}_S$ system is evaluated by numerically solving $\det[i\tilde{\mathcal{D}}_{(3)}^{-1}(p_0, \mathbf{0})] = 0$.

4. σ-B-$\bar{B}$-ω-B_{AS}-$\bar{B}_{AS}$ system

Here, we derive the mass formulas for the σ-B-$\bar{B}$-ω-B_{AS}-$\bar{B}_{AS}$ system. In this case, σ, B, $\bar{B}$ (or B^4, B^5) and the time components of ω, B_{AS}, $\bar{B}_{AS}$ (or V'^4, V'^5) can mix. In addition, the space components of ω, B_{AS}, $\bar{B}_{AS}$ (or V'^4, V'^5) also mix with each other.

First, we consider the mixing among σ, B, $\bar{B}$ (or B^4, B^5) and the time components of ω, B_{AS}, $\bar{B}_{AS}$. The inverse propagator of these six states at vanishing momentum $\boldsymbol{p} = \mathbf{0}$, $i\mathcal{D}_{(4)}^{-1}(p_0, \mathbf{0})$, is given by

$$i\mathcal{D}^{-1}_{(4)}(p_0,\mathbf{0}) = \begin{pmatrix} \mathcal{M}_{\sigma\sigma} & \mathcal{M}_{\sigma B_4} & \mathcal{M}_{\sigma B_5} & \mathcal{M}_{\sigma\omega} & \mathcal{M}_{\sigma V'_4} & \mathcal{M}_{\sigma V'_5} \\ \mathcal{M}_{B_4\sigma} & \mathcal{M}_{B_4B_4} & \mathcal{M}_{B_4B_5} & \mathcal{M}_{B_4\omega} & \mathcal{M}_{B_4V'_4} & \mathcal{M}_{B_4V'_5} \\ \mathcal{M}_{B_5\sigma} & \mathcal{M}_{B_5B_4} & \mathcal{M}_{B_5B_5} & \mathcal{M}_{B_5\omega} & \mathcal{M}_{B_5V'_4} & \mathcal{M}_{B_5V'_5} \\ \mathcal{M}_{\omega\sigma} & \mathcal{M}_{\omega B_4} & \mathcal{M}_{\omega B_5} & \mathcal{M}_{\omega\omega} & \mathcal{M}_{\omega V'_4} & 0 \\ \mathcal{M}_{V'_4\sigma} & \mathcal{M}_{V'_4B_4} & \mathcal{M}_{V'_4B_5} & \mathcal{M}_{V'_4\omega} & \mathcal{M}_{V'_4V'_4} & 0 \\ \mathcal{M}_{V'_5\sigma} & \mathcal{M}_{V'_5B_4} & \mathcal{M}_{V'_5B_5} & 0 & 0 & \mathcal{M}_{V'_5V'_5} \end{pmatrix}, \tag{C50}$$

where each matrix element reads

$$\mathcal{M}_{\sigma\sigma} = p_0^2 + \frac{C^2}{8}\bar{V}^2 - m_\sigma^2, \tag{C51}$$

$$\mathcal{M}_{\sigma B_4} = -\mathcal{M}_{B_4\sigma} = i\frac{C}{\sqrt{2}}\bar{V}p_0, \tag{C52}$$

$$\mathcal{M}_{\sigma B_5} = \mathcal{M}_{B_5\sigma} = -\frac{C}{\sqrt{2}}\bar{V}\mu_q - \frac{\lambda_2}{2}\sigma_0\Delta - \frac{C_3\bar{\omega}}{4}\bar{V}, \tag{C53}$$

$$\mathcal{M}_{\sigma\omega} = \mathcal{M}_{\omega\sigma} = \frac{C-C_3}{4}\bar{\omega}\sigma_0 - \frac{C_3}{4}\Delta\bar{V}, \tag{C54}$$

$$\mathcal{M}_{\sigma V'_4} = \mathcal{M}_{V'_4\sigma} = \frac{C+C_3}{4}\sigma_0\bar{V} - \frac{C}{\sqrt{2}}\Delta\mu_q - \frac{C_3}{4}\Delta\bar{\omega}, \tag{C55}$$

$$\mathcal{M}_{\sigma V'_5} = -\mathcal{M}_{V'_5\sigma} = i\frac{C}{2\sqrt{2}}\Delta p_0, \tag{C56}$$

$$\mathcal{M}_{B_4B_4} = p_0^2 + \frac{C^2}{8}\bar{V}^2 + \left(2\mu_q + \frac{C}{2\sqrt{2}}\bar{\omega}\right)^2 - m_{B_4}^2, \tag{C57}$$

$$\mathcal{M}_{B_4B_5} = -\mathcal{M}_{B_5B_4} = 2i\left(2\mu_q + \frac{C}{2\sqrt{2}}\bar{\omega}\right)p_0, \tag{C58}$$

$$\mathcal{M}_{B_4\omega} = -\mathcal{M}_{\omega B_4} = i\frac{C}{2\sqrt{2}}\Delta p_0, \tag{C59}$$

$$\mathcal{M}_{B_4V'_4} = -\mathcal{M}_{V'_4B_4} = -i\frac{C}{2\sqrt{2}}\sigma_0 p_0, \tag{C60}$$

$$\mathcal{M}_{B_4V'_5} = \mathcal{M}_{V'_5B_4} = \frac{C_3}{4}(\Delta\bar{V}_4 + \sigma_0\bar{\omega}) + \frac{C}{\sqrt{2}}\sigma_0\mu_q, \tag{C61}$$

$$\mathcal{M}_{B_5B_5} = p_0^2 + \left(2\mu_q + \frac{C}{2\sqrt{2}}\bar{\omega}\right)^2 - m_{B_5}^2, \tag{C62}$$

$$\mathcal{M}_{B_5\omega} = \mathcal{M}_{\omega B_5} = \sqrt{2}C\mu_q\Delta + \frac{C+C_3}{4}\Delta\bar{\omega} - \frac{C_3}{4}\sigma_0\bar{V}, \tag{C63}$$

$$\mathcal{M}_{B_5V'_4} = \mathcal{M}_{V'_4B_5} = \frac{C-C_3}{4}\Delta\bar{V} - \frac{C_3}{4}\sigma_0\bar{\omega} - \frac{C}{\sqrt{2}}\sigma_0\mu_q, \tag{C64}$$

$$\mathcal{M}_{B_5V'_5} = -\mathcal{M}_{V'_5B_5} = -i\frac{C}{2\sqrt{2}}\sigma_0 p_0, \tag{C65}$$

$$\mathcal{M}_{\omega\omega} = (m_\omega^t)^2, \tag{C66}$$

$$\mathcal{M}_{\omega V'_4} = \mathcal{M}_{V'_4\omega} = -\frac{C_3}{4}\sigma_0\Delta, \tag{C67}$$

$$\mathcal{M}_{V'_4V'_4} = (m_{V'_4}^t)^2, \tag{C68}$$

and

$$\mathcal{M}_{V'_5V'_5} = (m_{V'_5}^t)^2, \tag{C69}$$

with the mass parameters,

$$m_\sigma^2 = m_0^2 + \frac{\lambda_2}{4}(3\sigma_0^2 + \Delta^2) - \frac{C-C_3}{8}\bar{\omega}^2 - \frac{C-C^2+C_3}{8}\bar{V}^2, \tag{C70}$$

$$m_{B_4}^2 = m_0^2 + \frac{\lambda_2}{4}(\sigma_0^2 + \Delta^2) - \frac{C-C^2+C_3}{8}(\bar{V}^2 + \bar{\omega}^2), \tag{C71}$$

$$m_{B_5}^2 = m_0^2 + \frac{\lambda_2}{4}(\sigma_0^2 + 3\Delta^2) - \frac{C-C^2+C_3}{8}\bar{\omega}^2 - \frac{C-C_3}{8}\bar{V}^2, \tag{C72}$$

$$(m_\omega^t)^2 = m_1^2 + \frac{C}{8}(\sigma_0^2 + \Delta^2) - \frac{C_3}{8}(\sigma_0^2 - \Delta^2), \tag{C73}$$

$$(m_{V'_4}^t)^2 = m_1^2 + \frac{C}{8}(\sigma_0^2 + \Delta^2) + \frac{C_3}{8}(\sigma_0^2 - \Delta^2), \tag{C74}$$

and

$$(m^t_{V'_5})^2 = m_1^2 + \frac{C+C_3}{8}(\sigma_0^2+\Delta^2). \tag{C75}$$

In the presence of the mixing, the mass spectrum for the σ-B-$\bar{B}$ system is evaluated by numerically solving $i\mathcal{D}^{-1}_{(4)}(p_0,\mathbf{0})=0$.

Next, we consider the mixing among the spatial components of ω, B_{AS}, and $\bar{B}_{AS}$. In this case, the corresponding inverse propagator at vanishing momentum $\boldsymbol{p}=\mathbf{0}$, $i\tilde{\mathcal{D}}^{-1}_{(4)}(p_0,\mathbf{0})$, is given by

$$i\tilde{\mathcal{D}}^{-1}_{(4)}(p_0,\mathbf{0}) = \begin{pmatrix} \tilde{\mathcal{M}}_{\omega\omega} & \tilde{\mathcal{M}}_{\omega V'_4} & \tilde{\mathcal{M}}_{\omega V'_5} \\ \tilde{\mathcal{M}}_{V'_4\omega} & \tilde{\mathcal{M}}_{V'_4V'_4} & \tilde{\mathcal{M}}_{V'_4V'_5} \\ \tilde{\mathcal{M}}_{V'_5\omega} & \tilde{\mathcal{M}}_{V'_5V'_4} & \tilde{\mathcal{M}}_{V'_5V'_5} \end{pmatrix}, \tag{C76}$$

where each matrix element reads

$$\tilde{\mathcal{M}}_{\omega\omega} = -p_0^2 - \frac{g_\Phi^2}{2}\bar{V}^2 + (m^s_\omega)^2, \tag{C77}$$

$$\tilde{\mathcal{M}}_{\omega V'_4} = \tilde{\mathcal{M}}_{V'_4\omega} = -\frac{C_3}{4}\sigma_0\Delta + \sqrt{2}g_\Phi\bar{V}\mu_q + \frac{g_\Phi^2}{2}\bar{V}\bar{\omega}, \tag{C78}$$

$$\tilde{\mathcal{M}}_{\omega V'_5} = -\tilde{\mathcal{M}}_{V'_5\omega} = \sqrt{2}ig_\Phi\bar{V}p_0, \tag{C79}$$

$$\tilde{\mathcal{M}}_{V'_4V'_4} = -p_0^2 - \left(2\mu_q + \frac{g_\Phi}{\sqrt{2}}\bar{\omega}\right)^2 + (m^s_{V'_4})^2, \tag{C80}$$

$$\tilde{\mathcal{M}}_{V'_4V'_5} = -\tilde{\mathcal{M}}_{V'_5V'_4} = -2i\left(2\mu_q + \frac{g_\Phi}{\sqrt{2}}\bar{\omega}\right)p_0, \tag{C81}$$

and

$$\tilde{\mathcal{M}}_{V'_5V'_5} = -p_0^2 - \frac{g_\Phi^2}{2}\bar{V}^2 - \left(2\mu_q + \frac{g_\Phi}{\sqrt{2}}\bar{\omega}\right)^2 + (m^s_{V'_5})^2, \tag{C82}$$

with the mass parameters,

$$(m^s_\omega)^2 = m_1^2 + \frac{C}{8}(\sigma_0^2+\Delta^2) - \frac{C_3}{8}(\sigma_0^2-\Delta^2), \tag{C83}$$

$$(m^s_{V'_4})^2 = m_1^2 + \frac{C}{8}(\sigma_0^2+\Delta^2) + \frac{C_3}{8}(\sigma_0^2-\Delta^2), \tag{C84}$$

and

$$(m^s_{V'_5})^2 = m_1^2 + \frac{C+C_3}{8}(\sigma_0^2+\Delta^2). \tag{C85}$$

In the presence of the mixing, the mass spectrum for the ω-B_{AS}-$\bar{B}_{AS}$ system is evaluated by numerically solving $\det[i\tilde{\mathcal{D}}^{-1}_{(4)}(p_0,\mathbf{0})]=0$.

APPENDIX D: MASSES IN THE HADRONIC PHASE

As derived in Appendix C, in general, the hadron masses are evaluated by pole positions of the appropriate propagator matrices, which would be obtained numerically. When we focus on the hadronic phase, the mass formulas can be evaluated analytically. In this appendix, we exhibit the resultant mass formulas for all hadrons.

Such formulas can simply be obtained by taking $\Delta=0$ and accordingly $\bar{\omega}=\bar{V}=0$, while keeping $\sigma_0\neq 0$, in the mass formulas in Appendix C. In this limit, one can find

$$m^{(\mathrm{H})}_\omega = m^{(\mathrm{H})}_\rho = \sqrt{m_1^2 + \frac{C-C_3}{8}(\sigma_0^{(\mathrm{H})})^2}, \tag{D1}$$

$$m^{(\mathrm{H})}_{f_1} = m^{(\mathrm{H})}_{a_1} = \sqrt{m_1^2 + \frac{C+C_3}{8}(\sigma_0^{(\mathrm{H})})^2}, \tag{D2}$$

$$\begin{aligned} m^{(\mathrm{H})}_{B_S} &= m^{(\mathrm{H})}_\omega - 2\mu_q, \\ m^{(\mathrm{H})}_{\bar{B}_S} &= m^{(\mathrm{H})}_\omega + 2\mu_q, \end{aligned} \tag{D3}$$

$$\begin{aligned} m^{(\mathrm{H})}_{B_{\mathrm{AS}}} &= m^{(\mathrm{H})}_{f_1} - 2\mu_q, \\ m^{(\mathrm{H})}_{\bar{B}_{\mathrm{AS}}} &= m^{(\mathrm{H})}_{f_1} + 2\mu_q, \end{aligned} \tag{D4}$$

for the spin-1 hadrons, while

$$m^{(\mathrm{H})}_\pi = Z_\pi\sqrt{m_0^2 + \frac{\lambda_2}{4}(\sigma_0^{(\mathrm{H})})^2}, \tag{D5}$$

$$m^{(\mathrm{H})}_\eta = Z_\eta\sqrt{m_0^2 + \frac{\lambda_2}{4}(\sigma_0^{(\mathrm{H})})^2}, \tag{D6}$$

$$m^{(\mathrm{H})}_{a_0} = \sqrt{m_0^2 + \frac{3\lambda_2}{4}(\sigma_0^{(\mathrm{H})})^2}, \tag{D7}$$

$$m^{(\mathrm{H})}_\sigma = \sqrt{m_0^2 + 3\frac{\lambda_2}{4}(\sigma_0^{(\mathrm{H})})^2}, \tag{D8}$$

$$\begin{aligned} m^{(\mathrm{H})}_B &= m^{(\mathrm{H})}_\pi - 2\mu_q, \\ m^{(\mathrm{H})}_{\bar{B}} &= m^{(\mathrm{H})}_\pi + 2\mu_q, \end{aligned} \tag{D9}$$

$$\begin{aligned} m^{(\mathrm{H})}_{B'} &= m^{(\mathrm{H})}_{a_0} - 2\mu_q, \\ m^{(\mathrm{H})}_{\bar{B}'} &= m^{(\mathrm{H})}_{a_0} + 2\mu_q, \end{aligned} \tag{D10}$$

for the spin-0 hadrons. In Eqs. (D6) and (D5), the renormalization factors Z_π and Z_η are defined by

$$Z_\pi = \left(1 - \frac{C^2(\sigma_0^{(\mathrm{H})})^2}{8(m_{a_1}^{(\mathrm{H})})^2}\right)^{-1/2},$$
$$Z_\eta = \left(1 - \frac{C^2(\sigma_0^{(\mathrm{H})})^2}{8(m_{f_1}^{(\mathrm{H})})^2}\right)^{-1/2}, \tag{D11}$$

which stems from the π-a_1 mixing and the η-f_1 mixing, respectively. It should be noted that $Z_\pi = Z_\eta$ follows from $m_{f_1}^{(\mathrm{H})} = m_{a_1}^{(\mathrm{H})}$. These types of mixing originate from the spontaneous breakdown of chiral symmetry since $Z_\pi = Z_\eta = 1$ when $(\sigma_0^{(\mathrm{H})}) = 0$, as in the three-color eLSM [72].

[1] Jeremy W. Holt, Mannque Rho, and Wolfram Weise, Chiral symmetry and effective field theories for hadronic, nuclear and stellar matter, Phys. Rep. **621**, 2 (2016).
[2] V. Metag, M. Nanova, and E. Ya. Paryev, Meson–nucleus potentials and the search for meson–nucleus bound states, Prog. Part. Nucl. Phys. **97**, 199 (2017).
[3] Gert Aarts, Introductory lectures on lattice QCD at nonzero baryon number, J. Phys. Conf. Ser. **706**, 022004 (2016).
[4] Keitaro Nagata, Finite-density lattice QCD and sign problem: Current status and open problems, Prog. Part. Nucl. Phys. **127**, 103991 (2022).
[5] Shin Muroya, Atsushi Nakamura, Chiho Nonaka, and Tetsuya Takaishi, Lattice QCD at finite density: An introductory review, Prog. Theor. Phys. **110**, 615 (2003).
[6] Simon Hands, John B. Kogut, Maria-Paola Lombardo, and Susan E. Morrison, Symmetries and spectrum of SU(2) lattice gauge theory at finite chemical potential, Nucl. Phys. B **558**, 327 (1999).
[7] J. B. Kogut, D. K. Sinclair, S. J. Hands, and S. E. Morrison, Two color QCD at nonzero quark number density, Phys. Rev. D **64**, 094505 (2001).
[8] Simon Hands, Istvan Montvay, Luigi Scorzato, and Jonivar Skullerud, Diquark condensation in dense adjoint matter, Eur. Phys. J. C **22**, 451 (2001).
[9] Shin Muroya, Atsushi Nakamura, and Chiho Nonaka, Behavior of hadrons at finite density: Lattice study of color SU(2) QCD, Phys. Lett. B **551**, 305 (2003).
[10] Shailesh Chandrasekharan and Fu-Jiun Jiang, Phase-diagram of two-color lattice QCD in the chiral limit, Phys. Rev. D **74**, 014506 (2006).
[11] Simon Hands, Seyong Kim, and Jon-Ivar Skullerud, Deconfinement in dense 2-color QCD, Eur. Phys. J. C **48**, 193 (2006).
[12] Simon Hands, Peter Sitch, and Jon-Ivar Skullerud, Hadron spectrum in a two-colour baryon-rich medium, Phys. Lett. B **662**, 405 (2008).
[13] Simon Hands, Seyong Kim, and Jon-Ivar Skullerud, A quarkyonic phase in dense two color matter?, Phys. Rev. D **81**, 091502 (2010).
[14] Seamus Cotter, Pietro Giudice, Simon Hands, and Jon-Ivar Skullerud, Towards the phase diagram of dense two-color matter, Phys. Rev. D **87**, 034507 (2013).
[15] Simon Hands, Seyong Kim, and Jon-Ivar Skullerud, Non-relativistic spectrum of two-color QCD at non-zero baryon density, Phys. Lett. B **711**, 199 (2012).
[16] Tamer Boz, Seamus Cotter, Leonard Fister, Dhagash Mehta, and Jon-Ivar Skullerud, Phase transitions and gluodynamics in 2-colour matter at high density, Eur. Phys. J. A **49**, 87 (2013).
[17] V. V. Braguta, E. M. Ilgenfritz, A. Yu. Kotov, A. V. Molochkov, and A. A. Nikolaev, Study of the phase diagram of dense two-color QCD within lattice simulation, Phys. Rev. D **94**, 114510 (2016).
[18] M. Puhr and P. V. Buividovich, Numerical study of non-perturbative corrections to the chiral separation effect in quenched finite-density QCD, Phys. Rev. Lett. **118**, 192003 (2017).
[19] Tamer Boz, Ouraman Hajizadeh, Axel Maas, and Jon-Ivar Skullerud, Finite-density gauge correlation functions in QC2D, Phys. Rev. D **99**, 074514 (2019).
[20] N. Yu. Astrakhantsev, V. G. Bornyakov, V. V. Braguta, E. M. Ilgenfritz, A. Yu. Kotov, A. A. Nikolaev, and A. Rothkopf, Lattice study of static quark-antiquark interactions in dense quark matter, J. High Energy Phys. 05 (2019) 171.
[21] Kei Iida, Etsuko Itou, and Tong-Gyu Lee, Two-colour QCD phases and the topology at low temperature and high density, J. High Energy Phys. 01 (2020) 181.
[22] Jonas Wilhelm, Lukas Holicki, Dominik Smith, Björn Wellegehausen, and Lorenz von Smekal, Continuum Goldstone spectrum of two-color QCD at finite density with staggered quarks, Phys. Rev. D **100**, 114507 (2019).
[23] P. V. Buividovich, D. Smith, and L. von Smekal, Numerical study of the chiral separation effect in two-color QCD at finite density, Phys. Rev. D **104**, 014511 (2021).
[24] Kei Iida, Etsuko Itou, and Tong-Gyu Lee, Relative scale setting for two-color QCD with $N_f = 2$ Wilson fermions, Prog. Theor. Exp. Phys. **2021**, 013B05 (2021).
[25] N. Astrakhantsev, V. V. Braguta, E. M. Ilgenfritz, A. Yu. Kotov, and A. A. Nikolaev, Lattice study of thermodynamic properties of dense QC_2D, Phys. Rev. D **102**, 074507 (2020).
[26] V. G. Bornyakov, V. V. Braguta, A. A. Nikolaev, and R. N. Rogalyov, Effects of dense quark matter on gluon propagators in lattice QC_2D, Phys. Rev. D **102**, 114511 (2020).
[27] P. V. Buividovich, D. Smith, and L. von Smekal, Electric conductivity in finite-density $SU(2)$ lattice gauge theory with dynamical fermions, Phys. Rev. D **102**, 094510 (2020).
[28] P. V. Buividovich, D. Smith, and L. von Smekal, Static magnetic susceptibility in finite-density $SU(2)$ lattice gauge theory, Eur. Phys. J. A **57**, 293 (2021).
[29] Kei Iida and Etsuko Itou, Velocity of sound beyond the high-density relativistic limit from lattice simulation of

dense two-color QCD, Prog. Theor. Exp. Phys. **2022**, 111B01 (2022).
[30] Kotaro Murakami, Etsuko Itou, and Kei Iida, Chemical potential (in)dependence of hadron scatterings in the hadronic phase of QCD-like theories and its applications, J. High Energy Phys. 02 (**2024**) 152.
[31] Victor V. Braguta, Phase diagram of dense two-color QCD at low temperatures, Symmetry **15**, 1466 (2023).
[32] J. B. Kogut, Misha A. Stephanov, and D. Toublan, On two color QCD with baryon chemical potential, Phys. Lett. B **464**, 183 (1999).
[33] J. B. Kogut, Misha A. Stephanov, D. Toublan, J. J. M. Verbaarschot, and A. Zhitnitsky, QCD—like theories at finite baryon density, Nucl. Phys. B **582**, 477 (2000).
[34] J. T. Lenaghan, F. Sannino, and K. Splittorff, The superfluid and conformal phase transitions of two color QCD, Phys. Rev. D **65**, 054002 (2002).
[35] K. Splittorff, D. Toublan, and J. J. M. Verbaarschot, Diquark condensate in QCD with two colors at next-to-leading order, Nucl. Phys. B **620**, 290 (2002).
[36] Claudia Ratti and Wolfram Weise, Thermodynamics of two-colour QCD and the Nambu Jona-Lasinio model, Phys. Rev. D **70**, 054013 (2004).
[37] Gao-feng Sun, Lianyi He, and Pengfei Zhuang, BEC-BCS crossover in the Nambu-Jona-Lasinio model of QCD, Phys. Rev. D **75**, 096004 (2007).
[38] Kenji Fukushima and Kei Iida, Larkin-Ovchinnikov-Fulde-Ferrell state in two-color quark matter, Phys. Rev. D **76**, 054004 (2007).
[39] Tomas Brauner, Kenji Fukushima, and Yoshimasa Hidaka, Two-color quark matter: U(1)(A) restoration, superfluidity, and quarkyonic phase, Phys. Rev. D **80**, 074035 (2009); **81**, 119904(E) (2010).
[40] Takuya Kanazawa, Tilo Wettig, and Naoki Yamamoto, Chiral Lagrangian and spectral sum rules for dense two-color QCD, J. High Energy Phys. 08 (2009) 003.
[41] Masayasu Harada, Chiho Nonaka, and Tetsuro Yamaoka, Masses of vector bosons in two-color dense QCD based on the hidden local symmetry, Phys. Rev. D **81**, 096003 (2010).
[42] Jens O. Andersen and Tomas Brauner, Phase diagram of two-color quark matter at nonzero baryon and isospin density, Phys. Rev. D **81**, 096004 (2010).
[43] Tian Zhang, Tomas Brauner, and Dirk H. Rischke, QCD-like theories at nonzero temperature and density, J. High Energy Phys. 06 (2010) 064.
[44] Lianyi He, Nambu-Jona-Lasinio model description of weakly interacting Bose condensate and BEC-BCS crossover in dense QCD-like theories, Phys. Rev. D **82**, 096003 (2010).
[45] Nils Strodthoff, Bernd-Jochen Schaefer, and Lorenz von Smekal, Quark-meson-diquark model for two-color QCD, Phys. Rev. D **85**, 074007 (2012).
[46] Shotaro Imai, Hiroshi Toki, and Wolfram Weise, Quark-hadron matter at finite temperature and density in a two-color PNJL model, Nucl. Phys. A **913**, 71 (2013).
[47] Nils Strodthoff and Lorenz von Smekal, Polyakov-quark-meson-diquark model for two-color QCD, Phys. Lett. B **731**, 350 (2014).
[48] Naseemuddin Khan, Jan M. Pawlowski, Fabian Rennecke, and Michael M. Scherer, The phase diagram of QC2D from functional methods, arXiv:1512.03673.
[49] Dyana C. Duarte, P. G. Allen, R. L. S. Farias, Pedro H. A. Manso, Rudnei O. Ramos, and N. N. Scoccola, BEC-BCS crossover in a cold and magnetized two color NJL model, Phys. Rev. D **93**, 025017 (2016).
[50] Jingyi Chao, Phase diagram of two-color QCD matter at finite baryon and axial isospin densities, Chin. Phys. C **44**, 034108 (2020).
[51] Prabal Adhikari, Soma B. Beleznay, and Massimo Mannarelli, Finite density two color chiral perturbation theory revisited, Eur. Phys. J. C **78**, 441 (2018).
[52] Romain Contant and Markus Q. Huber, Dense two-color QCD from Dyson-Schwinger equations, Phys. Rev. D **101**, 014016 (2020).
[53] Daiki Suenaga and Toru Kojo, Gluon propagator in two-color dense QCD: Massive Yang-Mills approach at one-loop, Phys. Rev. D **100**, 076017 (2019).
[54] T. G. Khunjua, K. G. Klimenko, and R. N. Zhokhov, The dual properties of chiral and isospin asymmetric dense quark matter formed of two-color quarks, J. High Energy Phys. 06 (2020) 148.
[55] T. G. Khunjua, K. G. Klimenko, and R. N. Zhokhov, Influence of chiral chemical potential $\mu 5$ on phase structure of the two-color quark matter, Phys. Rev. D **106**, 045008 (2022).
[56] Toru Kojo and Daiki Suenaga, Thermal quarks and gluon propagators in two-color dense QCD, Phys. Rev. D **103**, 094008 (2021).
[57] Daiki Suenaga and Toru Kojo, Delineating chiral separation effect in two-color dense QCD, Phys. Rev. D **104**, 034038 (2021).
[58] Toru Kojo and Daiki Suenaga, Peaks of sound velocity in two color dense QCD: Quark saturation effects and semi-short range correlations, Phys. Rev. D **105**, 076001 (2022).
[59] Daiki Suenaga, Kotaro Murakami, Etsuko Itou, and Kei Iida, Probing the hadron mass spectrum in dense two-color QCD with the linear sigma model, Phys. Rev. D **107**, 054001 (2023).
[60] Mamiya Kawaguchi and Daiki Suenaga, Fate of the topological susceptibility in two-color dense QCD, J. High Energy Phys. 08 (2023) 189.
[61] Kotaro Murakami, Daiki Suenaga, Kei Iida, and Etsuko Itou, Measurement of hadron masses in 2-color finite density QCD, Proc. Sci. LATTICE2022 (**2023**) 154.
[62] Kotaro Murakami, Daiki Suenaga, Etsuko Itou, and Kei Iida (to be published).
[63] Yohei Kawakami and Masayasu Harada, Analysis of $\Lambda_c(2595)$, $\Lambda_c(2625)$, $\Lambda_b(5912)$, $\Lambda_b(5920)$ based on a chiral partner structure, Phys. Rev. D **97**, 114024 (2018).
[64] Yohei Kawakami and Masayasu Harada, Singly heavy baryons with chiral partner structure in a three-flavor chiral model, Phys. Rev. D **99**, 094016 (2019).
[65] Masayasu Harada, Yan-Rui Liu, Makoto Oka, and Kei Suzuki, Chiral effective theory of diquarks and the $U_A(1)$ anomaly, Phys. Rev. D **101**, 054038 (2020).
[66] Yonghee Kim, Emiko Hiyama, Makoto Oka, and Kei Suzuki, Spectrum of singly heavy baryons from a chiral effective theory of diquarks, Phys. Rev. D **102**, 014004 (2020).
[67] Yohei Kawakami, Masayasu Harada, Makoto Oka, and Kei Suzuki, Suppression of decay widths in singly heavy

baryons induced by the $U_A(1)$ anomaly, Phys. Rev. D **102**, 114004 (2020).
[68] Daiki Suenaga and Atsushi Hosaka, Novel pentaquark picture for singly heavy baryons from chiral symmetry, Phys. Rev. D **104**, 034009 (2021).
[69] Daiki Suenaga and Atsushi Hosaka, Decays of Roper-like singly heavy baryons in a chiral model, Phys. Rev. D **105**, 074036 (2022).
[70] Daiki Suenaga and Makoto Oka, Axial anomaly effect on the chiral-partner structure of diquarks at high temperature, Phys. Rev. D **108**, 014030 (2023).
[71] Hiroto Takada, Daiki Suenaga, Masayasu Harada, Atsushi Hosaka, and Makoto Oka, Axial anomaly effect on three-quark and five-quark singly heavy baryons, Phys. Rev. D **108**, 054033 (2023).
[72] Denis Parganlija, Peter Kovacs, Gyorgy Wolf, Francesco Giacosa, and Dirk H. Rischke, Meson vacuum phenomenology in a three-flavor linear sigma model with (axial-)vector mesons, Phys. Rev. D **87**, 014011 (2013).
[73] Daiki Suenaga and Phillip Lakaschus, Comprehensive study of mass modifications of light mesons in nuclear matter in the three-flavor extended linear σ model, Phys. Rev. C **101**, 035209 (2020).
[74] J. D. Walecka, A theory of highly condensed matter, Ann. Phys. (N.Y.) **83**, 491 (1974).